LATVIAN JOURNAL of PHYSICS and TECHNICAL SCIENCES

ISSN 0868 - 8257

4

(Vol. 56)

2019

SATURS

CONTENTS

СОДЕРЖАНИЕ

LATVIAN JOURNAL of PHYSICS and TECHNICAL SCIENCES

LATVIJAS FIZIKAS un TEHNISKO ZINĀTŅU ŽURNĀLS

ЛАТВИЙСКИЙ ФИЗИКО-ТЕХНИЧЕСКИЙ ЖУРНАЛ

Published six times a year since February 1964
Iznāk sešas reizes gadā kopš 1964. gada februāra
Выходит шесть раз в год с февраля 1964 года

4 (Vol. 56) • 2019

RĪGA

INDEKSĒTS (PUBLICĒTS) | INDEXED (PUBLISHED) IN

www.scopus.com
www.sciendo.com
EBSCO (Academic Search Complete, www.epnet.com), INSPEC (www.iee.org.com).
VINITI (www.viniti.ru), Begell House Inc/ (EDC, www.edata-center.com).

Izdevēji: Fizikālās enerģētikas institūts, LU Cietvielu fizikas institūts
Reģistrācijas apliecība Nr. 000700221
Redakcija: Krīvu iela 11, Rīga, LV-1006
Tel. 67551732
e-pasts: ezerniec@edi.lv
Interneta adrese: www.fei-web.lv

sciendo

LATVIAN JOURNAL OF PHYSICS
AND TECHNICAL SCIENCES
2019, N 4

DOI: 10.2478/lpts-2019-0021

PHYSICAL AND TECHNICAL ENERGY PROBLEMS

GAS COMBUSTION EFFICIENCY ENHANCEMENT: APPLICATION STUDY OF INTENSE ELESTROSTATIC FIELD

O. Krickis[1], N. Zeltins[2]

[1] Riga Technical University,
Department of Heat and Power Engineering Systems,
6B Kipsalas Str., Riga, LV-1048, LATVIA
otto.krickis@gmail.com
[2] Riga Technical University,
Faculty of Power and Electrical Engineering, Institute of Power Engineering
12-1 Azenes Str., Riga, LV-1048, LATVIA

A number of international, European Union and Latvian legislative acts have been developed, which regulate the efficiency of gas combustion plants and greenhouse gas emissions in the atmosphere. These legislative acts require the development of new scientifically efficient methods for gas optimal combustion with a minor impact on the environment. In order to achieve such a goal, different methods can be used, but the most efficient is an intensive electrostatic field application to control combustion and harmful emission formation in premixed flames. In the framework of the current study, the authors developed a hybrid burner, which allowed generating an intensive electrostatic field with intensity of more than 1000 kV/m. The study also investigated the impact of such a field on the formation of harmful emissions, including CO_2 and flue gas temperature. The empirical results showed that an intensive DC electrostatic field generated inside of the burner had an impact on the flame shape, CO_2, NO_x emissions and flue gas temperature. In its turn, by applying an intensive pulsating electrostatic field (multivariable experiment) it was possible to achieve the reduction in NO_x, CO emissions with a simultaneous increase in flue gas temperature, which was related to combustion process efficiency enhancement.

Keywords*: electrostatic field, emissions, gas combustion, ionic wind*

1. INTRODUCTION

In the light of the studies carried out so far and global conclusions of scientists about climate change, a number of international, European Union and

Latvian legislative acts have been developed, which contribute to the development of novel methods for the combustible gas efficiency enhancement and greenhouse gas emission reduction in the atmosphere. Taking into account the need to ensure national energy independence, with the possibility of fuel diversification or the substitution of different fuel types with equivalent properties, it is particularly important to find technologies for efficient and environmentally friendly use of replacement fuels and to develop technologies that allow for economically efficient operation of combustion plants. Since more than half of all Latvian energy resources are consumed for heating and hot water supply, it is important to analyse energy consumption and the possibilities of reducing harmful emissions related to energy production [1].

The current research is devoted to an in-depth study of the combustion process under the influence of an electrostatic field by conducting laboratory experiments with full-scale equipment that excludes the effects of the surrounding environment on the subject. The results of the research can be used in the project of the Ministry of Economics of the Republic of Latvia "Trends, Challenges and Solutions of Latvian Gas Infrastructure Development (LAGAS)", project No. VPP-EM-INFRA-2018/1-0003.

2. INFLUENCE OF THE ELECTROSTATIC FIELD ON THE COMBUSTION PROCESS

The stability of combustion and the improvement of the boundaries of combustion are one of the most pressing issues for improvement of modern combustion plants. The use of an electrostatic field in the flame zone provides a solution that is simple in implementation and effective at the same time to change the flame structure and to control the concentration of harmful emissions in the flue gases. The electric field influences the combustion of the flame in three ways: by the thermal effect associated with the conversion of electric energy into heat; by the ionic wind effect; and by the electrically-chemical effect [2]. The electrically-chemical effect produces fast electrons, radicals, ionic and induced molecules before the combustion zone, which in turn greatly affects the chemistry of the flame [3]–[6]. Both laminar and turbulent combustion have shown a combustion improvement under the influence of an electric field (AC and DC) at low electricity consumption compared to the heat input in the combustion chamber. However, there are differences in the result, which make it difficult to identify the main physical phenomenon that contributes to improvement of combustion stabilization [7].

There are a number of chemical ionization reactions that constitute flame ion chemistry. The two most important chemical ionization reactions (1 and 2) are as follows:

$$CH + O \rightarrow CHO^{+} + e^{-}; \tag{1}$$

$$CH^{*} + C_2H_2 \rightarrow C_3H_3^{+} + e^{-}. \tag{2}$$

CH_3O^+ ion concentration in flame is 2–4 times lower compared to $C_3H_3^+$ ion. Ion $C_3H_3^+$ is considered to be the main one in the ion mechanism of the soot formation process. In addition, it should be noted that CHO^+ is a primary ion in a reaction between an oxidizing atom and a fuel before the combustion process [8].

According to scientists' studies in the reaction zone of the hydrocarbon flame, the chemical ionization process and subsequent reactions are associated with the positive ions of the charged particles (H_3O^+, $C_3H_3^+$, CH_3^+, CHO^+), the formation of negative ions (O_2^-, OH^-, O^-, CHO_2^-, CHO_3^-, CO_3^-) and electrons, which interact under the influence of *Coulomb* force resulting in their transformation and minimising the local electrical potential in which they are located [9], [10].

Using an electric field (E) to influence the combustion process, *Lorentz's* forces act on charged particles, causing them to accelerate. This calls the drift speed of directly directed charged particles [11]. The positive ions move in the direction of the cathode (lower potential electrode) and repeat the lines of the electric field while the electrons and negative ions move in the opposite direction of the anode (higher potential electrode). This movement of charged particles into a hydrocarbon flame creates an electrical current [12].

In the full-scale test organised by Latvian researchers, the application of an electric field to the industrial boiler DKVR-10-13 was analysed, which resulted in the improvement of heat output by 3.5–8.5 %, with an average increase in efficiency of the industrial boiler of 2.8 % at the simultaneous thermal NO_x reduction in the range of 15–20 % [13].

3. RESEARCH METHODOLOGY

In the framework of the current research, the investigational process was divided into two stages in order to identify the different type of the equipment layout and electrostatic field impact on the combustion process parameters and flue gas composition changes, which depend on one or more experimental factors.

The first stage of the research is based on gathered data from the previous study [14]. The experimental equipment included specially designed combustion chamber and burner (hereinafter – hybrid burner), an electric field-generator – laboratory-type transformer with a small voltage adjustment step, combining all of these parts with step-up high-voltage transformer with a high-voltage multiplier that simultaneously performed a rectification function. This stage of the research is based on the determination of changes in the composition of the flue gas, depending on the voltage of the DC source used, which was applied to the hybrid burner. The factor to be controlled for this experiment is the DC voltage, while the response is the concentration and temperature values of the components of the flue gas, which in total constitute the seven parameters. The limit of the variable factor is the voltage range from 0 V to 2200 V. The study was based on one factor variation at nine levels with manually performed distribution of levels.

In the framework of the second stage of the research, the authors performed the analysis of flue gas composition and flue gas temperature change of LPG (propane molar fraction 0.92) combustion process depending on the three external

variable factors: 1 – pulsating current (voltage); 2 – pulsating current frequency (switching frequency); 3 – ozone generation equipment operating interval (duration of the relay switch). An analysis of the interactions among the three variable factors was performed for each factor at ten levels. According to the assessment of the experiment design, the method developed by Latvian scientist Dr.sc.ing. V. Eglājs – Latin hypercube, which refers to the space-filling experiments, was chosen.

4. EXPERIMENTAL EQUIPMENT LAYOUT

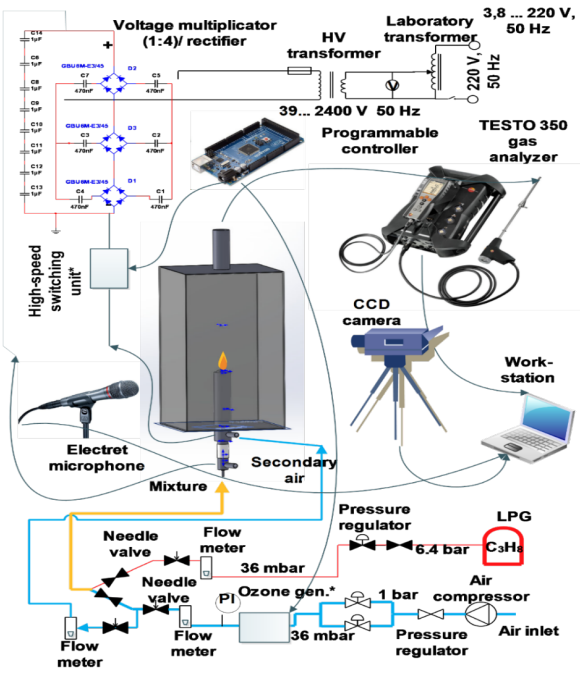

Fig. 1. Scheme of experimental equipment for the first and second stages of the research.

The experimental equipment used for the research consists of a number of individual components whose operation is synchronised in a single process and allows for the analysis of the measured data for a single mode. The experimental equipment (Fig. 1) has the following components: for flame shape visual analysis a monochrome CCD camera and high-speed camera were used, an industrial flue gas analyser (TESTO 350), a flame-sound recording device with a sound amplifier, a voltage regulation unit, a voltage multiplication and a current rectification unit, a high-voltage ignition unit, an air supply compressor, an air flow regulation and adjustment unit, an accounting unit, a fuel gas supply unit, a gas flow regulation and adjustment unit, a flow mixing unit, a combustion chamber with two-stage air flow decomposition and workstation for data processing. Apart from these components, a specially designed ozone gas generation device (including the Generation Time Control Module) was used during the second stage of the study. For the second stage of the research, a specially designed high-speed switching unit (with a high-voltage MOSFET type transistor) and an electronic four-channel oscilloscope were used.

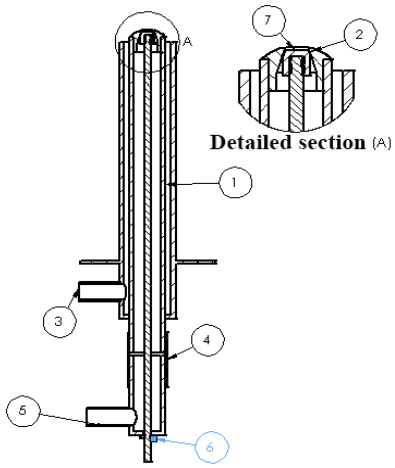

Fig. 2. Section view of the hybrid burner with element numbering:
1 – Air/Gas supply channel; 2 – Flow control unit/external electrode;
3 – Secondary air supply channel; 4 – Dielectric PVC sleeve; 5 – Air/Gas supply channel;
6 – Flow adjustment rod (burner-centring rod); 7 – profiled cap of the burners.

A hybrid burner (Fig. 2) was designed and developed for the research. It was made of stainless steel and used to generate an electric field by connecting a high-voltage source to it. For electric field generation, the burner construction included a number of dielectric elements to ensure the separation of the outer casing of the burner from the burner core, which in turn played the role of both the air/combustible gas mixture supply control and the flame shape adjustments function. The bottom and core of the burner were insulated from the upper burner shell with a PVC insert and dielectric (textolite) centring rings. The outer diameter of the centring rings is equal to the inner diameter of the burner's primary flow channel, while for the provision of flow in it 8 holes with a diameter of 3 mm were made. The geometry of the upper part of the core (cap) shall be closely adapted to the geometry of the upper part of the outer shell of the burner, thereby ensuring the radial discharge of the mixture into the combustion zone. The burner was designed to supply secondary air to the combustion zone (inside the combustion chamber) through a separate channel around the primary mixture channel. Such an equipment layout and air supply method allowed analysing the premixed flame combustion, which was constructively equivalent to the full-scale industrial burners' performance indicators.

The hybrid burner design developed during the research (Fig. 2) provided an effective intensity of the electrostatic field of 1140 *kV/m*, which several times exceeded the parameters of the equipment achieved in the studies of other scientists [15], [16].

5. RESEARCH RESULTS

The first stage of the research was based on the analysis of the impact of the intensive DC electrostatic field on the combustion of liquefied propane gas, including visual recording of the flame front, the analysis of changes in flue gas composition, as

well as the treatment of the thermo-acoustic signal using Fast Fourier Transformation (hereinafter – *FFT)* method.

At the first and second stages of the research, a combustion chamber of the same design was used, whereby, in addition to direct measurements, a numerical analysis of the combustion process was carried out using a simulation method based on realistic GRIMECH 3.0 and SAN DIEGO chemical-kinetic mechanisms in CHEMKIN-PRO environment. For this numerical analysis, actual recorded air and gas flows were used.

The results of the numerical analysis of the combustion process showed that the burner constructed within this research was capable to secure propane burning within a wide range of equivalence factors from to (determined by the proportion of fuel/air in the reactor zone), which was equivalent to the propane molar fraction range .

5.1. Results of the First Stage of the Research

The goal of the first stage of the research was to determine the effects of intense DC electrostatic field on gaseous fuel combustion, flame shape variation and flue gas formation. Under these conditions, the voltage range was increased, keeping all rest parameters unchanged. At this stage of the study, the fuel input capacity was 0.17 kW_{th}. As a reference point for flame-shape comparison, the authors used flame visual information taken in electrostatic free conditions. To determine the deviations of flame shape, the pictures were supplemented with the coordinates of the pixels. The maximum flame-consumed current was , when a positive potential was connected to the burner-centering rod. According to the voltage-current characteristics (Fig. 3), it is concluded that the consumed current significantly increases starting from 1300 *V*, when effect of ionic wind appears. These results have a good correlation with the picture set of flame-shape changes (Fig. 4).

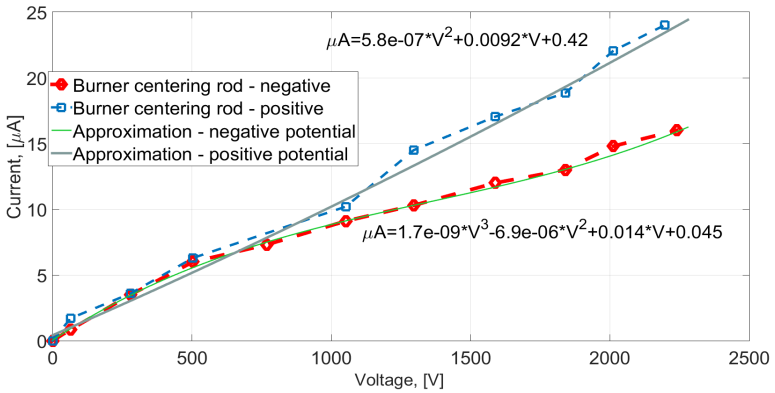

Fig. 3. Voltage-current characteristics of the experimental equipment.

According to the flame shape and length change analysis, it can be concluded that the electrostatic field impact on the flame shape with the negative connected potential to the burner-centring rod is minimal. This is due to a relatively small

surface area (12 mm^2) of the centring rod, which performed the function of the electrode. Taking into account that the electrode of the burner-centring rod was located below the root of the flame, the drift of the positive ions from the flame front to the negative electrode was practically unattainable. These results showed that such an arrangement of the electrode and the connection of a DC source contributed to a minimal change in flame shape compared to the combustion mode without the use of an electrostatic field.

According to the graphical results with the positive connected potential to the burner-centring electrode, it is apparent that starting from 400 *V* the length of the flame kernel is decreasing, while starting from 700 *V* there is an extension of the root of the flame. This could be explained with a positive ion drift to the burner shell, to which the negative potential was attached. The impact of the electrostatic field (Fig. 4) on the change in flame length is significant and its contraction is 24 % compared to the burning mode without the use of an electrostatic field. The flame root extension, however, is 27 %. These results show that an electrode with a diameter of 2.5 times larger than the flame diameter constitutes a proportional reduction in the length of the flame kernel and an extension of the root of the flame.

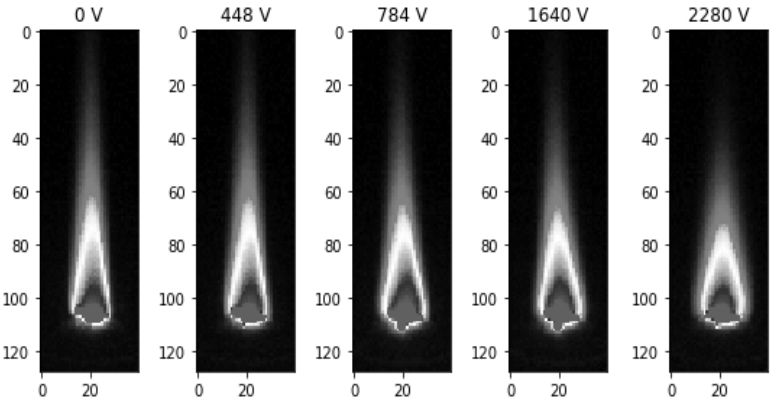

Fig. 4. Graphical comparison of the flame shape in the voltage range 0–2280 *V* when the burner-centring rod was used as an anode and the burner shell as a cathode.

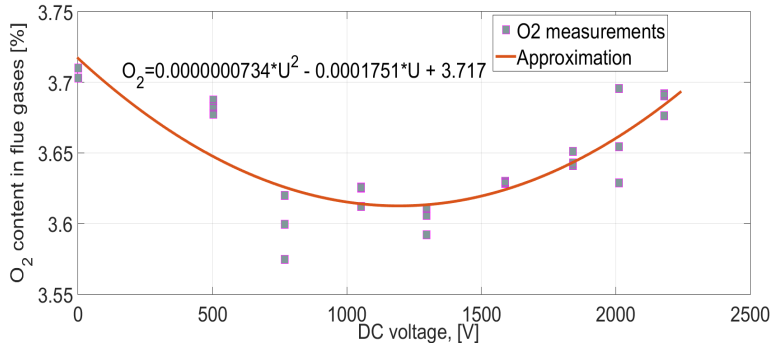

Fig. 5. The oxygen content in the flue gases under intense electrostatic field conditions, when the burner shell was used as a cathode.

In the framework of the research, the authors performed the analysis of the flue gas composition using a specially designed inspection point in the combustion chamber. The sampling point was created at the top of the vertical wall of the combustion chamber, which ensured the placement of the flue gas analyser TESTO 350 measuring probe perpendicular to the flue gas flow. The analysis covered the following parameters: percentage of oxygen in the flue gases O_2, concentration of carbon monoxide in the flue gases CO, carbon dioxide in the flue gases CO_2, concentration of nitrogen oxide in the flue gases NO, concentration of nitrogen dioxide in the flue gases of NO_2, concentration of nitrogen oxides in the flue gases NOx and flue gas temperature.

When the burner shell was used as an anode, an increase in oxygen content in the flue gases was observed, ranging from 4.14 % to 4.35 %. While in the second part of the experiment, when the burner shell was used as a cathode, the oxygen content in the voltage range 0–1300 V was reduced parabolically from 3.72 % to 3.6 %. From 1300 V oxygen content increased to its original state (Fig. 5).

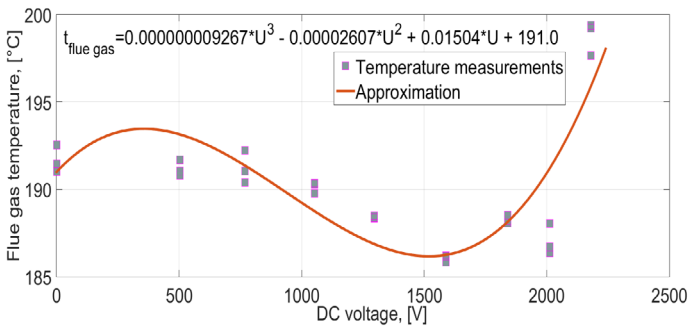

Fig. 6. Flue gas temperature under intense electrostatic field conditions, when the burner shell was used as a cathode.

Temperature of flue gas is directly proportional to the flame combustion temperature, up to which determination of the flame temperature changes was carried out based on flue gas temperature registration via a flue gas analyser probe with an integrated thermocouple.

According to the measurement results, when the burner shell was used as an anode, the temperature of flue gas evenly descended, which correlated with the oxygen content change in the flue gas. At the maximum electrostatic field intensity, a decrease in the flue gas temperature of 7.5 °C was noted, which was 3.5 % compared to the combustion mode without the use of an electrostatic field. In the experiment with a positive-connected potential to the burner-centring rod (the burner shell was used as a cathode), it was found that starting from 1300 V, the temperature of the flue gases began increasing parabolically, reaching its peak (199 °C) at a maximum electrostatic field strength of 1140 kV/m (Fig. 6).

The maximum specific increase in nitrogen oxides (NO_x) concentration was 10 % at 525 *kV/m* electrostatic field intensity (Fig. 7), when the burner shell was used as an anode. In these conditions, the maximum reduction in the concentration of carbon monoxide (CO) was 35 *mg/m*^{3}, which was equivalent to a specific reduction of 5.2 %.

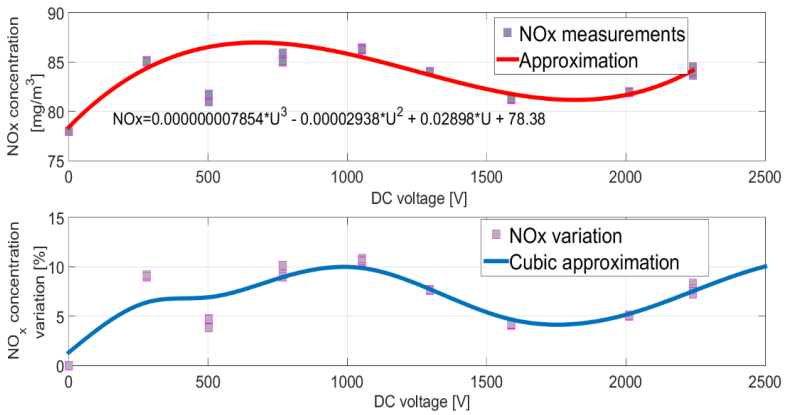

Fig. 7. Nitrogen oxide concentration variation under intense electrostatic field conditions, when the burner shell was used as an anode.

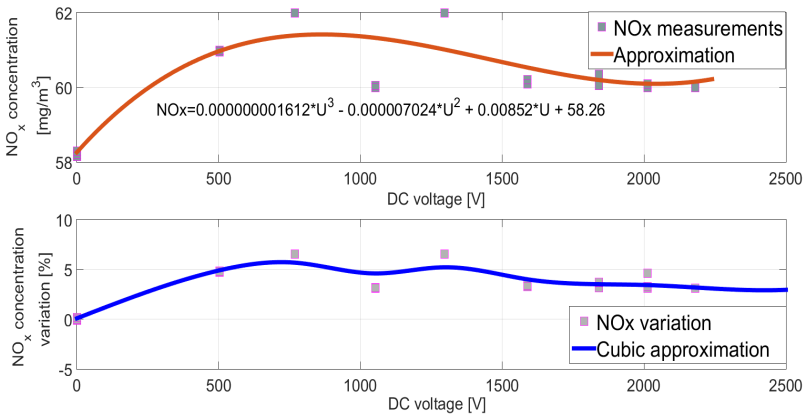

Fig. 8. Nitrogen oxide concentration variation under intense electrostatic field conditions, when the burner shell was used as a cathode.

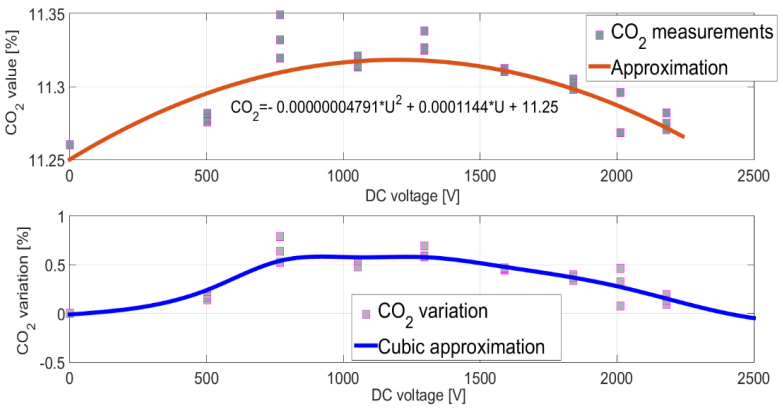

Fig. 9. Carbon dioxide concentration variation under intense electrostatic field conditions, when the burner shell was used as a cathode.

However, when the burner shell was used as a cathode and the burner-centring rod as an anode, the maximum increase in NO_x emissions was 5.3 % (Fig. 8), while the

reduction in CO emissions reached 7.1 % compared to the baseline. An improvement in the combustion process was found in an experiment with a positive connected potential to a burner-centring rod and simultaneous electrostatic field intensity of 525 kV/m, carbon dioxide (CO_2) in the flue gases increased by 0.07 %, which was equivalent to a specific increase of 0.6 % (Fig. 9).

The flame thermo-acoustic signal under the influence of the electrostatic field was analysed using the Electret type microphone for the sound range 0.02–16 *kHz*, which was placed at the same level with the average flame plane. Based on the processed acoustic signal results in the full frequency range 0.02–25 kHz, it can be concluded that no change in the amplitude of the acoustic flame signal is observed starting from 2 kHz. The fundamental recorded harmonic according to the *FFT* analysis of the acoustic signal is 150 *Hz*. It should be noted that the same fundamental harmonic was recorded at both variations of the DC polarity connection.

The *FFT* analysis shows that connection of DC positive potential to the burner-centring rod and the simultaneous connection of negative potential to the burner shell has a significant impact on the flame acoustic signal (noise) enhancement. According to the comparison of signal amplification at peak voltage (2280 *V*), the signal amplitude is 115 times higher compared to the baseline.

5.2. Results of the Second Stage of the Research

The goal of the second stage of the research was to determine the effects of intense pulsating electrostatic field including multivariate interaction on the composition of flame combustion products. The multivariate impact analysis was based on the analysis of the variation in the composition of the flue gases, depending on three factors: pulsating current voltage; pulsating current frequencies; switching intervals for the ozone generating device.

The maximum pulsating current voltage was limited to 900 *V*, a pulsating current frequency of 10,000 *Hz* and an operating interval of the ozone generating device of 2000 *ms*. Taking into account assessment of the safety and ozone leakage aspects, the ozone generating device was integrated into the air flow channel before mixing with the combustion gas.

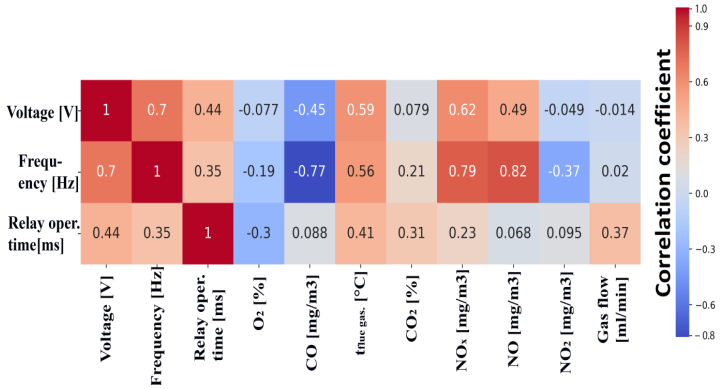

Fig. 10. Multivariate correlation heat map for an experiment with negative pulsating current potential connected to the burner-centring rod.

For a three-factor cross-impact analysis on a number of registered responses, a cross-correlation factor was established for each variable and each response. The calculated linear correlation factors for each factor and response were compiled in a graphic form using the heat map method. The results of this interaction analysis are presented in Figs. 10 and 11.

According to the results presented in Fig. 10, it can be concluded that none of the factors justified a linear correlation with the oxygen content in the flue gases. However, the study detected a significant impact of the pulsating current frequency on the change in carbon monoxide (CO) concentration. These results showed that a sequential substitution of oxygen by ozone gas using a negative-connected pulsating potential to the burner-centring rod did not have an impact on the measurements. It should be noted that this multivariate experiment showed the impact of the set frequency of a pulsating current on NO_x and NO emissions.

In an experiment with a positive pulsating current potential, which was connected to the burner-centring rod (Fig. 11), a good correlation was found between all three influence factors on the flue gas temperature and a change in NO_x concentration. The obtained results refer to the voltage range up to 900 *V*. The heat map of the correlation factors showed the existing relationship between the voltage and the concentration of NO_2 in the flue gases, as well as between the frequency of the pulsating current and the concentration of NO_2 in the flue gases. In addition, the change in CO concentration in the flue gases was mostly dependent on the conditions with increased voltage.

The assessment of the temperature change in the flue gases, depending on three factors, proved the high potential of the pulsating current and partial ozone gas application. Each step-up level of each factor increased the temperature of the flue gases. In addition, the results of the CO emission measurements testified about more complete combustion and better heat release from the flame.

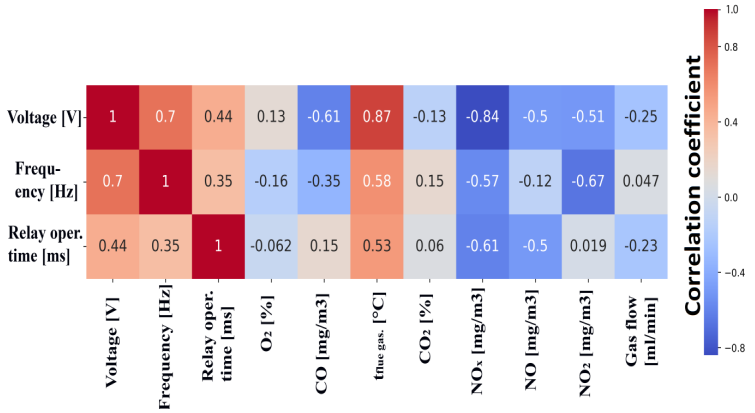

Fig. 11. Multivariate correlation heat map for experiment with positive pulsating current potential connected to the burner-centring rod.

On the basis of these results, it is concluded that the intensive electrostatic field of the pulsating current source, its pulse frequency, and the partial substitution of the oxidizer with a more active oxidising agent (ozone) improve the propane flame combustion and the heat release from the flame, which can be demonstrated by an

increase in the temperature of the flue gases. In the framework of the experiment, it was found that pulsating current voltage, pulsating frequency and ozone as oxidizer had a direct effect on the rapid NO_x formation process rather than on thermal NO_x.

6. CONCLUSIONS

The proposed method, using intensive DC and pulsating electrostatic field, for the gaseous fuel combustion enhancement allows increasing the efficiency of the combustion process and controlling the formation of harmful emissions in the atmosphere.

The study experimentally proved the intensive DC electrostatic field impact on flame shape changes, which began at intensity of 200 *kV/m*. At an electrostatic field intensity of the 1140 *kV/m* flame length reduction was 24 % and the extension of the flame root – 27 %. According to the results, the intensive DC electrostatic field increased NO_x emissions by 5.3 % on average, while the reduction in CO emissions reached 7.1 % compared to baseline. Experimentally analytical results showed that the intensive DC electrostatic field had an influence on the thermo-acoustic effect of the flame, significantly increasing the amplitude of the harmonics. The results suggested that the electrostatic field did not contribute to the acoustic resonant effect of the flame.

The results of the research also demonstrated that the pulsating current electrostatic field, combined with a sequential substitution of oxidizer (free oxygen and three atomic oxygen), allowed achieving NO_x emission reduction and was capable to increase the temperature of flue gases indicating the intensification of heat exchange.

The developed method can be adjusted to different gaseous fuels, thus ensuring better combustion capabilities and lower impact on the atmosphere. Moreover, it also allows controlling the geometry of flame, which can be used in order to reduce maintenance costs of the gas combustion equipment.

ACKNOWLEDGEMENTS

The research has been supported by the National Research Programme, project "Trends, Challenges and Solutions of Latvian Gas Infrastructure Development" (LAGAS) (No. VPP-EM-INFRA-2018/1-0003).

REFERENCES

1. Davis, A., Mikelsons, K., Puikevica-Puikevska, I., Silantjeva, I., Zebergs, V., & Zeltins, N. (2007). The methods of analysis for raising the energy efficiency and the reduction of greenhouse gases. In: *27th USAEE/IAEE North American Conference: Developing & Delivering Affordable Energy in the 21st Century* (pp. 24–25), USA, Houston, Texas, Book of extended abstracts.
2. Zhang, Y., Wu, Y., Yang, H., Zhang, H., & Zhu, M. (2013). Effect of high-frequency alternating electric fields on the behaviour and nitric oxide emission of laminar non-premixed flames. *Fuel*, *109*, 350–355, DOI: https://doi.org/10.1016/j.fuel.2012.12.083

3. Ombrello, T., Won, S.H., Ju, Y., & Williams, S. (2010). Flame propagation enhancement by plasma excitation of oxygen. Part I: Effects of O_3. *Combustion and Flame*, *157*(10), 1906–1915, DOI: https://doi.org/10.1016/j.combustflame.2010.02.005
4. Ombrello T., Won, S.H., Ju, Y., & Williams, S. (2010). Flame propagation enhancement by plasma excitation of oxygen. Part II: Effects of O_2 ($a^1\Delta$ g). *Combustion and flame*, *157*(10), 1916–1928, DOI: https://doi.org/10.1016/j.combustflame.2010.02.004
5. Sun, W., Uddi, M., Ombrello, T., Won, S.H., Carter, C., & Ju, Y. (2011). Effects of non-equilibrium plasma discharge on counterflow diffusion flame extinction. *Proceedings of the Combustion Institute, 33*(2), 3211–3218, DOI: https://doi.org/10.1016/j.proci.2010.06.148
6. Sun, W., Uddi, M., Won, S.H., Ombrello, T., Carter, C., Ju, Y. (2012). Kinetic effects of non-equilibrium plasma-assisted methane oxidation on diffusion flame extinction limits. *Combustion and Flame*, *159*(1), 221–229, DOI: https://doi.org/10.1016/j.combustflame.2011.07.008
7. Belhi, M., Domingo, P., & Vervisch, P. (2010). Direct numerical simulation of the effect of an electric field on flame stability. *Combustion and Flame, 157*(12), 2286–2297, DOI: https://doi.org/10.1016/j.combustflame.2010.07.007
8. Fialkov, A. B., Kalinich, K. Y., & Fialkov, B. S. (1992). Experimental determination of primary ions in flame. *Twenty-fourth Symposium on Combustion/The Combustion Institute*. Elsevier, 785–791, DOI: https://doi.org/10.1016/S0082-0784(06)80096-20
9. Goodings, J. M., Bohme, D. K., & Ng, C. W. (1979). Detailed ion chemistry in methane oxygen flames. I. Positive ions. *Combustion and Flame, 36*, 27–43, DOI: https://doi.org/10.1016/0010-2180(79)90044-0
10. Goodings, J. M., Bohme, D. K., & Ng, C. W. (1979). Detailed ion chemistry in methane oxygen flames. II. Negative ions. *Combustion and Flame*, *36*, 45–62, DOI: https://doi.org/10.1016/0010-2180(79)90045-2
11. Bisetti, F., & El Morsli, M. (2012). Calculation and analysis of the mobility and diffusion coefficient of thermal electrons in methane/air premixed flames. *Combustion and Flame*, *159*(12), 3518–3521, DOI: https://doi.org/10.1016/j.combustflame.2012.08.002
12. Hu, J., Rivin, B., & Sher, E. (2000). The effect of an electric field on the shape of co-flowing and candle-type methane-air flames. *Experimental Thermal and Fluid Science*, *21*(1–3), 124–133, DOI: https://doi.org/10.1016/S0894-1777(99)00062-X
13. Barmina, I., Purmalis, M., Valdmanis, R., & Zaķe, M. (2016). Electrodynamic control of the combustion characteristics and heat energy production. *Combustion Science and Technology*, *188*(2), 190–206.
14. Krickis, O. (2017). Effect of electric field in the stabilized premixed flame on combustion process emissions. In: *IOP Conference Series: Materials Science and Engineering. IOP Publishing*, *251*, 1–5, DOI: https://doi.org/10.1088/1757-899X/251/1/012116
15. Gan, Y., Luo, Y., Wang, M., Shi, Y., & Yan, Y. (2015). Effect of alternating electric fields on the behaviour of small-scale laminar diffusion flames. *Applied Thermal Engineering*, *89*, 306–315, DOI: https://doi.org/10.1016/j.applthermaleng.2015.06.041
16. Belhi, M., Domingo, P., & Vervisch, P. (2009). Effect of electric field on flame stability. *Proc. of the European Combustion Meeting*, *1*, 1–6.

GĀZES DEGŠANAS EFEKTIVITĀTES UZLABOŠANA: INTENSĪVĀ ELEKTROSTATISKĀ LAUKA LIETOŠANAS PĒTĪJUMS

O. Krickis, N. Zeltiņš

K o p s a v i l k u m s

Rakstā apskatīta zinātniski pamatota metode gāzveida kurināmā optimālākai sadegšanai, pielietojot intensīvu elektrostatisko lauku. Pētījuma ietvaros tika izstrādāta un aprobēta unikālās konstrukcijas gāzes sadedzināšanas iekārta, kas ļauj ģenerēt elektrostatisko lauku ar intensitāti, pārsniedzot 1000 kV/m. Rezultātā tika izpētīta līdzstrāvas, kā arī pulsējošās strāvas elektrostatiskā lauka ietekme uz gāzes kurināmā degšanu, īpaši vērtējot liesmas formas izmaiņas, dūmgāžu sastāva variāciju un degšanas efektivitāti.

12.07.2019.

sciendo

LATVIAN JOURNAL OF PHYSICS
AND TECHNICAL SCIENCES
2019, N 4

DOI: 10.2478/lpts-2019-0022

CHALLENGES AND BARRIERS BY TRANSITION TOWARDS 4TH GENERATION DISTRICT HEATING SYSTEM: A STRATEGY TO ESTABLISH A PRICING MECHANISM

U. Osis, N. Talcis, J. Ziemele*
JSC "Rigas Siltums", Cesu Str. 3A, Riga, LV-1012, LATVIA
*e-mail: jelena.ziemele@rs.lv

Transition of the district heating (DH) system to the 4th generation system involves several challenges, which refer not only to the introduction of state-of-art technologies, but also to the development of a sustainable pricing methodology. Introduction of the 4th generation systems will soon force the DH industry to solve issues regarding the possibility of organisation of the market in the same way as it happened in the power industry (Directive 2009/72/EC) by complete separation of producers from the transmission system service providers. The present article discusses various development scenarios of a DH utility within the framework of an organised market and their pricing methodologies, as well as evaluates their sustainability considering the transition to the 4th generation system.

Keywords: *4th generation district heating, heat tariff, pricing mechanism*

1. INTRODUCTION

Gradual transition from the 3rd to the 4th generation systems is taking place in the district heating (DH) systems in Europe and elsewhere in the world where they are developed [1]. This is related to the necessity to modify the conditions of operation of the district heating systems and to shift emphasis to new technological solutions in heat sources [2], networks and at the consumers' side [3] in order to secure their competitiveness and to prevent harm to the environment. At the same time, DH utilities are following the European Union (EU) guidelines and are implementing the requirements stipulated by the EU laws and regulations developed for the purpose of contributing to prevention of the global climate change [4]. In 2008, the EU Commission set the goal to reduce the greenhouse gas (GHG) emissions by 20 % by 2020 in comparison to 1990 [5]. Considering the fact that 64 % of energy consumption in Europe is used for space heating and hot water production [6], district heating has a high potential in the decarbonisation process. In order to attain the set climate goals, the 4th generation district heating (4GDH) systems are based on renewable energy sources, heat transmission takes place by using smart thermal grid and low-temperature networks and the system as a whole is a part of

the smart energy system [7]. Introduction of the 4th generation systems will soon force the DH industry to solve issues regarding the possibility of organisation of the market in the same way as it happened in the power industry (Directive 2009/72/EC) [8] by complete separation of producers from the transmission system service providers, which means free access of third parties to the system and competition among producers [9].

The goal of the DH system is to provide the necessary amount of heat to households, commercial and industrial customers by implementing modern and sustainable district heating technologies, to secure their competitiveness, security and high quality service for customers. Nowadays DH systems are integrated in many countries in Europe and North America.

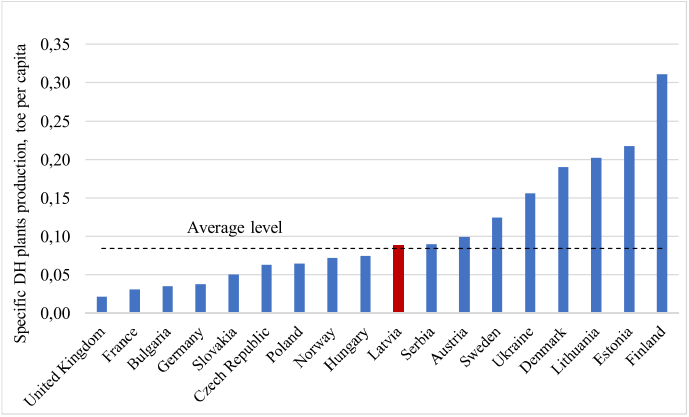

Fig. 1. Specific heat production in 2016 for different European countries [10].

The specific heat production per capita in 18 European countries is presented in Fig. 1, which clearly demonstrates the presence of the DH system in all the Baltic countries. The mean specific heat production amounts to 0.084 toe per capita and this level is exceeded by Latvia, Lithuania and Estonia and a few Scandinavian countries: Sweden, Denmark and Finland.

A modern DH system should be sustainable, competitive and secure. The above-listed criteria both compete among themselves and supplement each other. Coordinated interaction of the above-mentioned criteria secure the advantages of the DH system compared to individual and decentralised heat supply [11]. DH systems possess numerous advantages, which justly allow them to expand in the countries where they are present and develop in the countries where they have not been popular until now, for example, in the UK [12]. The price or tariff of heat, as it is referred to on a regulated market, is among the main parameters describing competitiveness of each DH system. The parameters, which affect the operation of the DH system or the heat tariff, can be grouped in several categories:

- Technological parameters: the volume of consumed heat and the consumption profile, the length of DH networks, the consumption density [13];
- Environment and climate parameters: emissions and use of natural resources, the share of renewable energy resources, use of low potential heat [14];

- Economic parameters: fuel and electricity prices [15], tax payments, specific investments in technologies [16];
- Institutional parameters: standards of building efficiency, heat and power generating plants, policy instruments for implementation of various measures [17];
- Social parameters: sufficiency of heat for households, arrangement of the city environment [18].

Improvement of efficiency at consumers, by implementing energy efficiency measures, installing heat insulation of buildings and implementing innovative projects (passive buildings or buildings as a heat storage) [19], is among the most important factors forcing a DH utility to plan its operations in advance and affecting heat costs [20].

On a regulated DH market, which exists in many post-soviet countries, the heat price is determined by the eligible costs of the DH utility. In this case, the law also defines the profit margin. This method is referred to as the cost-plus method. On a deregulated market, the marginal cost method is used and it is based on the costs of one additional energy unit. None of the pricing methods is perfect and industry experts often propose various improvements and additions thereto [21].

Irrespective of the fact that many studies have been devoted to the heat tariff, various pricing methodologies and their impact upon the DH system sustainability, competitiveness and security have been insufficiently analysed. The study is aimed at defining the tariff changes and their development trends by identifying the factors affecting tariff changes under different DH system development scenarios for transition to the 4th generation system and analysing the possibility of maintaining the competitiveness of the DH system.

2. METHODOLOGY

The methodology comprises several steps. Within the first step, for the purpose of evaluating various alternatives of the DH system development, the mathematic model of the district heating systems was developed describing the stages of heat production, transmission and consumption (Fig. 2 Section A) by means of a system of mathematic equations (1).

$$\begin{cases} Q_{con} = Q_{prod} - Q_{los} \\ Q_{con} = Gc\Delta t \\ Q_{los} = T\lambda F\Delta t_{log} = T\sum_{n=1}^{j} q_{losj}L_{i,} \\ Q_{prod} = \eta B Q_{LHV} \\ N_{ee} = Tg\rho G_s H/\eta_p \end{cases} \quad (1)$$

where Q_{con} – heat received by the consumer, MWh/year; Q_{prod} – heat produced by DH company; G – amount of heat carrier, m^3/year; c – volume specific heat capacity, MWh/m^{3}K ; Δt – temperature difference, K; λ – heat conductivity coefficient, MW/(m^{2}K); F – pipe surface, m^2; Δt_{log} – logarithmic temperature difference, K; L – thermal

length, m; B – fuel consumption, kg/year; Q_{LHV} – lower calorific value of the fuel, MWh/kg; q_{losj} – linear heat losses (MW/m); L_i – length of heat network segment (m), j – total number of pipe network segments; T – hours per time period (h/year); g – gravitational acceleration (m/s^2); ρ – heat carrier density (kg/m^3); η_p – efficiency of pump (-); H – total pressure drop (m); N_{ee} – electricity consumption, Wh/year; – amount of heat carrier, m^3/s.

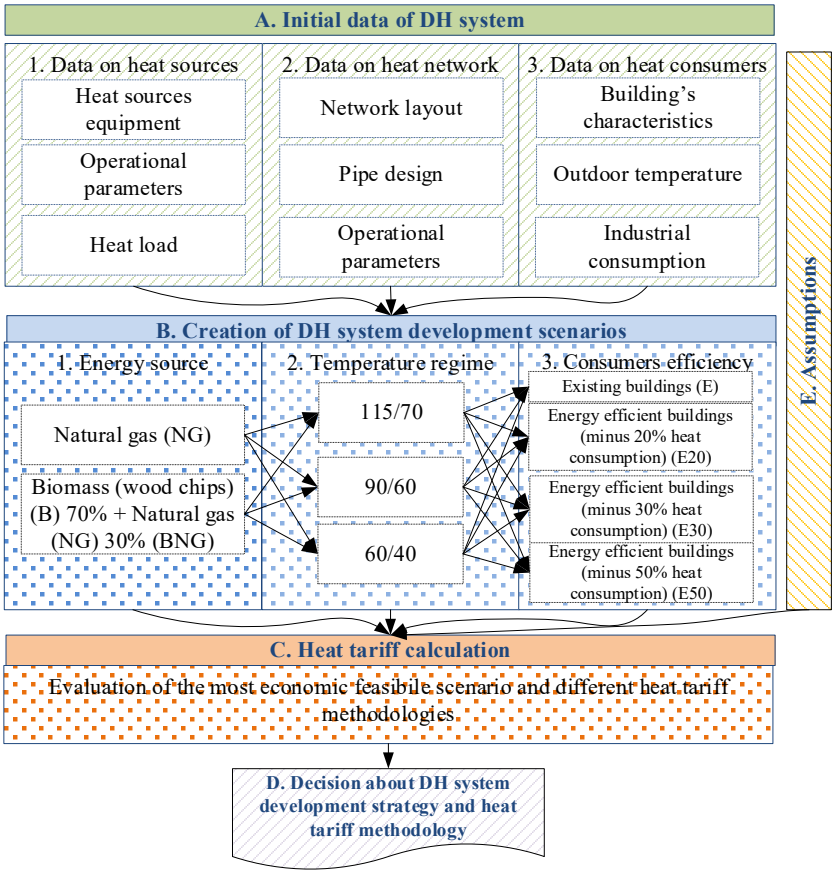

Fig. 2. Conceptual scheme of the study methodology.

In order to optimise the work and costs, each DH utility should have a task of minimising fuel consumption, heat losses and power consumption for pumping the heat carrier.

$$\begin{cases} B \rightarrow min \\ Q_{los} \rightarrow min. \\ N_{ee} \rightarrow min \end{cases} \quad (2)$$

The mathematic model developed within the first step of the methodology allows identifying these values.

Within the next step of the study, 28 estimation scenarios of the DH system were developed (Fig. 2, Section B), potentially describing the development of situations in DH utilities in the cities and villages in Latvia. It was taken into account that many DH systems were producing heat by suing natural gas at the beginning of the 21st century and then it was gradually replaced by renewable energy sources (biomass). Moreover, the process affecting development of the DH system is related to improvement of energy efficiency of buildings. Therefore, development scenarios whereby energy efficiency of buildings improves gradually by 20, 30 and 50 % were studied in the present article.

In the third step of the study, heat tariffs T consisting of one part or two parts (€/MWh) were estimated for all the scenarios in compliance with the methodology approved in the Republic of Latvia [22]. The single component tariff consists of three parts and is expressed by the following equation:

$$T = T_{prod} + T_{tr} + T_{sale}, \tag{3}$$

where: T_{prod} – production tariff, €/MWh; T_{th} – transmission tariff, €/MWh; T_{sale} – sale tariff, €/MWh.

Each of the tariff parts comprises the amounts of fixed and variable costs. For example, the production tariff is determined as follows:

$$T_{prod} = \frac{(VC_R + FC_R)}{Q_{prod}}, \tag{4}$$

where VC_R – variable costs of the production tariff, €/yr; FC_R – fixed costs of the production tariff, €/yr; Q_{prod} – produced heat, MWh/yr.

The variable costs of the production tariff consist of the sum of several components:

$$VC_R = Q_{prod}\left(\frac{C_{fuel}}{\eta} + C_{taxR} + C_{el}Q_{prod}^{el} + C_{othR}\right), \tag{5}$$

where VC_R – variable costs of the production tariff, €/yr; Q_{prod} – produced heat, MWh/yr; C_{fuel} – fuel price, €/MWh; η – efficiency rate of the technology; C_{taxR} – taxes, €/MWh; C_{el} – electricity price, €/MWh; Q_{prod}^{el} – electricity consumption for production needs, MWh_{el}/MWh_{th},; C_{othR} – other production costs, €/MWh.

The share of variable costs in the sales tariff is low; however, the fixed costs are calculated in the same way for all the tariff parts.

$$FC_i = Q_{prod}C_{M\&R} + \frac{C_{eq}N_N}{\tau_{cr}} + C_{pr} + C_s + C_{ins} + C_{othi}, \tag{6}$$

whereFC_i – fixed costs of the tariff, €/yr; i – selected part of the tariff (production, transmission or sale tariff); Q_{prod} – produced heat, MWh/yr; $C_{M\&R}$ – plant repair and maintenance costs, €/MWh; C_{eq} – costs of technologies, €/MW; N_N – installed capacity of the technology, MW; τ_{cr} – loan repayment period, yr; C_{pr} – loan interest repayment, €/yr; Cs – wages including social insurance contributions, €/yr; C_{ins} – insurance costs, €/yr; C_{othR} – other costs, €/yr.

In case of the tariff consisting of two parts, all the costs in each DH system stage (production, transmission and sale) are divided into two components: payment for consumed heat T_1 and fixed payment T_2. The heat transmission and distribution tariff is determined based on the following equation:

$$T_{1i} = \frac{VC_i}{Q_{con}}. \tag{7}$$

On top of that, there is a fixed fee for demanded capacity:

$$T_{2i} = \frac{FC_i}{N_N}. \tag{8}$$

The main simulation assumptions are related to the costs of fuel and electricity, as well as the price of the particular installed technology and operational costs. The estimations were made at the mean natural gas price of 21 €/MWh, the price of wood chips of 17.80 €/MWh and the electricity end price of 110 €/MWh in Latvia (Fig. 2, section E).

In the course of analysis of the transition to the 4GDH, also the possibility of integration of the quality component, which is present in several calculation methodologies in the Scandinavian countries and determine the temperature difference of the heat carrier in the supply and the return, was reviewed. Considering that on a deregulated market the heat tariffs are defined by applying the method of marginal costs, particular variable costs of different scenarios with their marginal costs were compared within the study. Marginal costs (*MC*) represent the increase of the total costs (*VC*) if the production volume changes by one unit:

$$MC = \frac{dVC}{dQ_{prod}} + \frac{dFC}{dQ_{prod}}, \tag{9}$$

where *VC* – variable cost, *FC* – fixed cost, and Q_{prod} – the quantity of production. In addition, it is necessary to take into account that fixed costs do not change short-term and then the component dFC/dQ_{prod} is equal to zero.

Within the study, the tariffs of all the scenarios were analysed considering their sustainability and the maintenance of the competitiveness of the DH system, as well as borders were defined where the system expansion would be desirable (attraction of new customers). In addition, strengths and weaknesses of various heat-pricing methodologies were assessed by testing them under different DH system

development scenarios for transition to the 4GDH.

3. CASE STUDY

District heating systems in Latvia and also in the other Baltic countries have been historically well developed (Fig. 1). Natural gas was used as the basic fuel at the end of the last century and at the beginning of this century. As the costs of fossil fuel increased and Latvia also assumed obligations to reduce CO_2 emissions, the use of wood fuel gradually increased. Figure 3 presents the share of fossil and renewable fuel in the DH sector during the last five years.

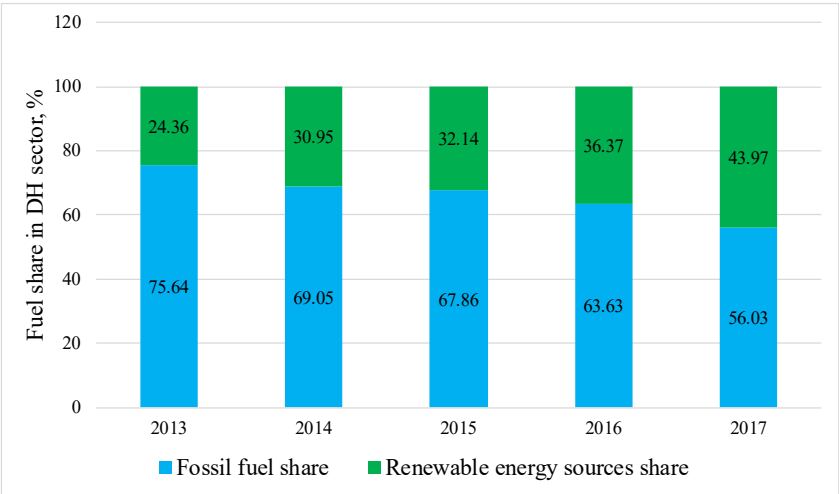

Fig. 3. Fossil and renewable fuel share in the DH sector.

It should be noted that the ratio of renewable energy sources (wood chips) into the total fuel balance has increased over the past years, especially in heat sources that are based only on the boiler technology. In 2017, they used 76.3 % of wood in comparison to cogeneration plants where the share of use of wood was lower and accounted for 37.6 % this year [23].

The goals of development and modernisation of the DH system are defined by the EU legislation, and on the national level the strategy and the means for attaining them are selected. The EU Strategy on Heating and Cooling [9] provides for direction of DH system towards the 4th generation systems based on the use of renewable energy resources, low-temperature heat supply and utilisation of highly efficient technological solutions. The business model of DH systems differs by country. In Latvia, several market participants are interested in development of the DH system: the state, municipalities, the DH utility, new project developers, households and corporate consumers. Municipalities play an important role in development and implementation of the general DH concept. Several 4GDH projects have been implemented in the EU in close cooperation with municipalities [24]. In Latvia, heat supply is provided by using different options: the municipality supplies heat to its residents by performing the functions of the DH utility; this is done by a private DH utility or both options are combined whereby the municipality, a state institution

and a private utility form a joint stock company. In this case, the municipality and the state institution perform two functions, in particular – take care of secure and profitable heat supply and provide the legal regulation of the system.

The methodology developed within the present article was tested in a DH district located in Riga. Heat supply there is provided to 32 buildings with the total floor area of 53,000 m^2. Heat is produced by natural gas fired boilers with the installed capacity of 2 x 2.5 MW equipped with condensation economisers. The temperature schedule 115/70 was maintained in DH networks. The average heat consumption during the last 5 years was 8820 MWh per year (70 % is consumed by households and 30 % is consumed by industrial consumers). The total length of the DH networks in the system is approximately 3,300 m (supply). Supplied heat is consumed for space heating and hot water production.

4. RESULTS AND DISCUSSION

4.1. Transition towards 4GDH: Possibilities, Bottlenecks, and Challenges

Transition to the 4GDH system is related to the necessity to provide heat supply to buildings with high efficiency by transiting to a low-temperature schedule in DH networks allowing for reduction of heat losses in the networks and integration of low potential heat sources [1]. The transition involves not only technological innovations, but also the necessity to perform institutional and organisational structural changes in the DH sector in order to provide suitable cost and motivation structure. The heat tariff is among the most important indices describing the efficiency of the DH system.

Fig. 4 (in Section 1) summarises the factors that affect the technological solutions of the DH system and therefore influence the total costs. It is a historically accepted practice that the DH system should be based on a high security back-up. As a result, higher capacity generating plants are installed, the temperature regime in the networks is higher than needed and this contributes to the increase of heat production costs (Figure 4, Section 1, Maintenance & repair costs, Depreciation costs, and DH system efficiency).

Transition to the 4GDH system makes one assess the system reserve in order to reduce heat losses and investment costs. When new buildings are constructed, projects comprise modern solutions of heating elements (floor or wall heating). Heat substations should be equipped with appropriate low-temperature schedule heat exchange surfaces (Fig. 4, Section 1 – Consumers).

Fuel costs are among the most important parameters, which have substantial impact upon the heat costs. As it was emphasised before, the 4GDH is based on diversification of used fuel and transition to domestic renewable energy resources (Fig. 4, Section 2 – Production). Use of renewable energy resources contributes to a positive impact upon:

- development possibilities on the regional and local scale;
- employment opportunities;
- energy independence and secure energy supply;
- use of modernised energy technologies;
- reduction of GHG emissions.

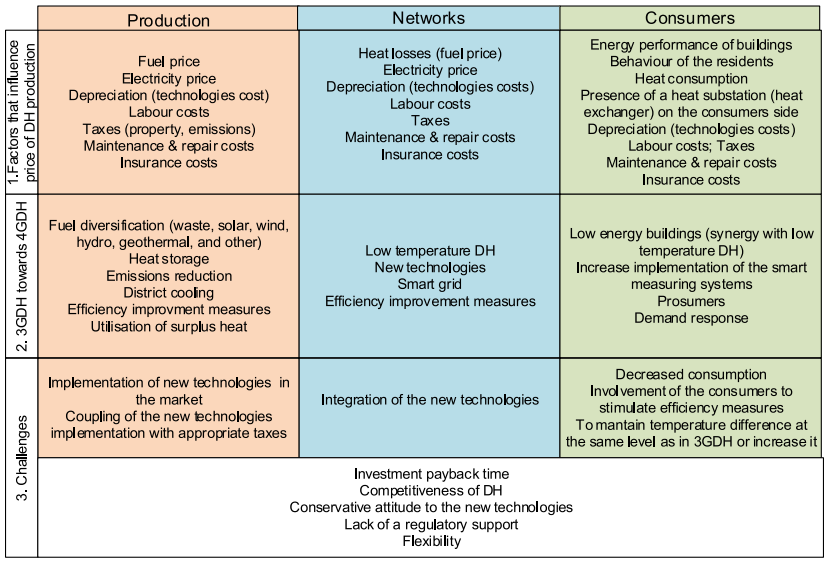

Fig. 4. Transition towards 4GDH: possibilities, bottlenecks, and challenges.

Many studies focus on the introduction of the low-temperature schedule in DH networks [25], [26], where various positive aspects of their implementation are evaluated [27]:

- Higher efficiency in distribution networks since heat losses are lower;
- The possibility of using plastic pipes in distribution networks with low operation pressure;
- The reduced supply temperatures also reduce the risk of water boiling in the network, i.e., resulting in a lower risk of two-phase flow in pumps.

In the International Energy Agency report, transition processes to a low temperature in the DH are divided into two stages [28]. At the first stage, the temperature potential in the current DH system is reduced by using the current system potential and compensating the efficiency measures at the consumer's side. Consequently, if consumers replace windows, the energy consumption is reduced. Within the second stage, by making capital investment, longer thermal lengths should be used in substation heat exchangers or some devices of heat substations should be replaced (regulators, heat exchangers). All measures for reduction the current temperature levels used in DH systems need to be developed by a coherent modernisation process and must be coordinated by DH company.

Consumers who produce part of heat or electricity and who are referred to as prosumers also play their role within the 4GDH (Fig. 4, Section 2, Consumers). Small-scale production of heat is generally less efficient in comparison to the

DH system [19]. New challenges to consumers are caused by the demand side management when consumers modify their consumption profile by transferring consumption from peak hours to another time, thus the consumers' heat demand can be satisfied by a lower installed capacity and savings of capital investments can be obtained [29]. Integration of renewable energy resources is related to the necessity to develop heat storage because energy generation and consumption profiles do not coincide on the time scale, which generally improves the system flexibility.

The lack of know-how and experience of introduction of new technologies consisting of hybrid systems when several technologies are used at the same time (CHP, HP, solar systems and other) creates a barrier for their implementation in Latvia (Fig. 4, Section 3, Production, Networks).

Development of new technologies requires considerable investment and often, within a regulated market, the available resources are limited in DH utilities. Therefore, it would be desirable that the state and the municipal taxation policy is favourable for innovation.

Maintenance of competitiveness of the DH system is an important factor from the point of view of economy and environment. The economic profitability of the DH system presents an opportunity to attain lower costs and to provide lower tariffs to consumers [30]. There are several factors serving as reasons for the above: the possibility to produce heat and generate electricity at the same time [31]; to use modern technologies and the most profitable fuel at all DH stages [32]; to integrate surplus heat [33]; to use the advantages presented by economies of scale.

4.2. Heat Tariff Development Methodology

As several authors have pointed out, the heat pricing methodologies are obsolete and do not correspond to the actual market situation [34]. Irrespective of that DH utilities operate under the same conditions within a single national regulated market, often there are considerable differences of tariffs. Therefore, researchers and industry experts propose different methods of defining heat tariffs. For example, there is a proposal to introduce benchmarking in order to restrict the possibility for DH utilities to increase their costs [35], or to use the incremental cost method, which considers not only the marginal costs of the existing system, but also its replacement costs (the incremental cost method) [36].

4.2.1. Development of Low-Temperature Network. The Cost of Heat Energy Distribution

Transition of the current DH system to a low-temperature schedule depends on several factors that describe this system, in particular, the network length, the heat load density, the possibility of consumers to switch to a low-temperature schedule.

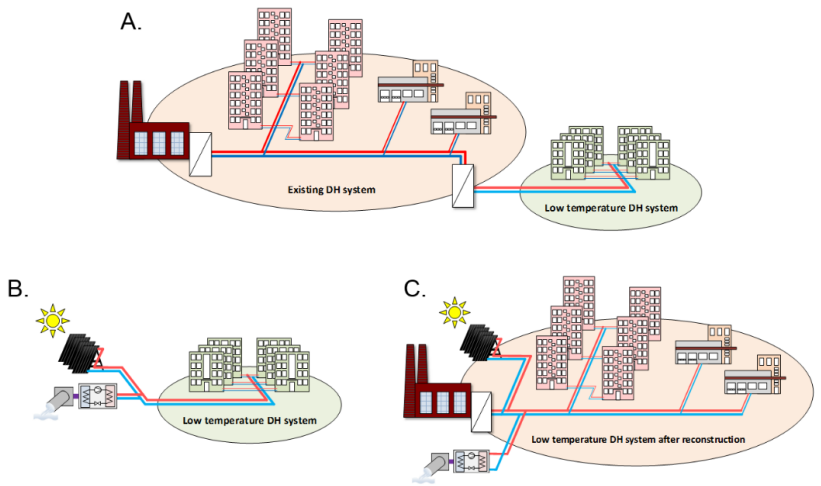

Fig. 5. Options of connection of a low-temperature DH district.

Thanks to the advantages of the low-temperature heat supply system, several EU DHs have got involved in the introduction of low-temperature heat supply. Transition to low-temperature heat supply can be done both within an existing heat supply system and by constructing a new system. The following three scenarios are possible for implementing low-temperature heat supply:

- Connection of low-temperature districts to an existing system through sectioning it by using a heat exchanger and creating two hydraulic circuits (Fig. 5, Version A). In this case, new consumers or reconstructed houses may be connected.
- Another option is to create low-temperature DH systems by constructing new districts when the heating systems of buildings are originally designed as low-temperature systems with floor heating or low-temperature heating elements (Fig. 5, Version B).
- Coherent modernisation of the current system and transition to a low-temperature system (Fig. 5, Version C).

The technical performance of the connection point to the existing DH networks can be different [37], for example, mixing of return water with supply water, increase of the return water temperature potential by means of economizers, condensers, heat pumps and other solutions.

The present article focuses on the study of the DH system, which is modernised in a coherent manner (Version C) and at the same time, by transition to the low temperature, the efficiency in buildings is improved and 70 % of natural gas is replaced by wood fuel.

Operational parameters of different development scenarios of DH systems are presented in Table 1.

Losses of the transmission system for scenarios where natural gas is used as fuel are presented in Fig. 6, which shows that transition to lower temperature schedules reduces losses in the networks allowing for reduction of operational expenditure.

Table 1

Heat Distribution Parameters for Different Development Scenarios

Scenarios	Produced heat, MWh/yr	Consumed heat, MWh/yr	Heat losses, MWh/yr	Electricity consumption, MWh/yr	Heat load, MW
E-115/70-NG E-115/70-BNG	8828	7977	851	103	3.99
E20-115/70-NG E20-115/70-BNG	7233	6381	851	88	3.19
E30-115/70-NG E30-115/70-BNG	6435	5584	851	80	2.79
E50-115/70-NG E50-115/70-BNG	4840	3988	851	65	1.99
E-90/60-NG E-90/60-BNG	8700	7977	723	107	3.99
E20-90/60-NG E20-90/60-BNG	7105	6381	723	90	3.19
E30-90/60-NG; E30-90/60-BNG	6307	5584	723	83	2.79
E50-90/60-NG E50-90/60-BNG	4712	3988	723	68	1.99
E-60/40-NG E-60/40-BNG	8540	7977	563	115	3.99
E20-60/40-NG E20-60/40-BNG	6945	6381	563	98	3.19
E30-60/40-NG E30-60/40-BNG	6147	5584	563	90	2.79
E50-60/40-NG E50-60/40-BNG	4552	3988	563	73	1.99

For example, expenditure for transmission (heat losses and electricity consumption of pumping of the heat carrier) will be reduced by 22 % by transition from the temperature schedule 115/70 to 60/40 in existing buildings.

However, it is necessary to take into account that transition to lower temperature schedules is compatible with improvement of building efficiency at the consumer's side. Reduction of heat consumption by 20 % and transition to the temperature schedule 60/40 (E20-60/40-NG) allows reducing transmission expenses only by 2 % (A compared to B). As the heat reduction at the consumer's side increases, transmission costs get relatively higher compared to the initial situation (A compared to C, D, E)). Furthermore, in all the cases transmission costs are relatively lower at the temperature schedule 60/40.

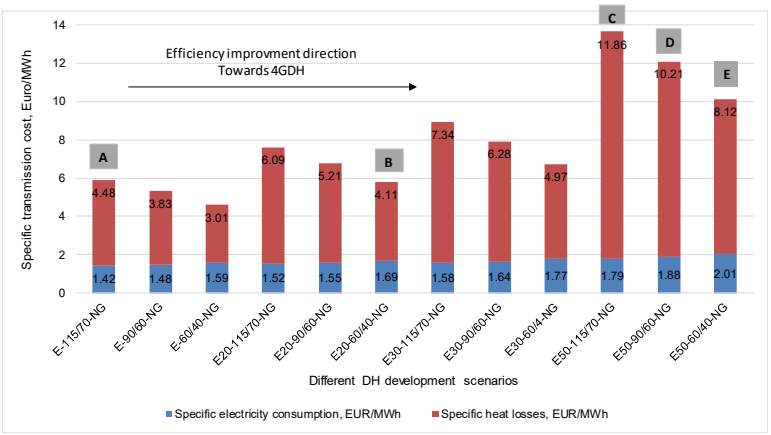

Fig. 6. Specific distribution costs for different scenarios (the natural gas price 21 €/MWh; the electricity price 110 €/MWh), where 115/70, 90/60 and 60/40 – the temperature regime in the DH network, NG – natural gas, E – existing building, E20, E30, E50 – buildings with improved efficiency to a specific level.

4.2.2. One- and Two-Part Tariff Evaluation for the Developed Scenarios

By using the equations defined in the Methodology Section (from (3) to (6)), the one-part tariff was estimated for 28 created scenarios described in Section 3.

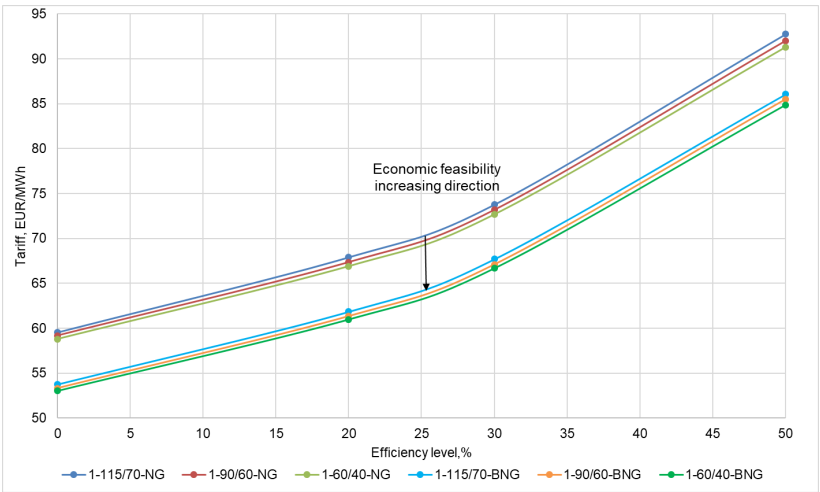

Fig. 7. The one-part tariff development for all the scenarios reviewed by the study (115/70, 90/60 and 60/40 – the temperature regime in the DH network, NG – natural gas, 1 – one-part heat tariff).

As the consumption decreases by more than 20 %, it is necessary to take into account that the heat tariff will increase sharply (Fig. 7). If it was 59.53 €/MWh under the initial scenario, as the heat consumption decreased by 50 %, the tariff would increase to 92.75 €/MWh, which would be 55.8 % above the initial tariff. Transition to the renewable energy resource (biomass) allows the DH utility to partially compensate an increase in the tariff, and by a decrease in consumption

to 50 % and transition to a lower temperature schedule (60/40) the heat tariff will be 84.86 €/MWh, which will be 42.6 % above the initial tariff. Lower losses in the network and lower transmission costs contribute to an additional decrease of 13.2% in the total tariff. Each heat supply utility is interested in installation of innovative technologies allowing for reduction of costs. In case when the DH utility uses boilers for heat production, the fuel price has the largest impact upon the tariff. Thus, if a competitive fuel is selected, there is a possibility to partially compensate for an increase in the tariff.

Sven Werner [4] emphasises that municipal DH utilities traditionally prefer the cost-oriented methodology for setting tariffs and obtaining the profit guaranteed by the law. Upon transition to the 4GDH system, the pricing methodology should be changed to ensure that it encourages not only introduction of innovations in DH utilities, but also technological modifications at the consumer's side. As heat consumption in the current DH system decreases, the specific fixed costs of the utility will increase (FC/Q_{con}, €/MWh). Therefore, the DH company is interested in changing to a two-part tariff. Considering the fact that improvement of energy efficiency at the consumer's side is taking place in Latvia, though at a slow pace, several heat supply utilities are considering this opportunity. This possibility is envisaged by the current heat pricing methodology [22]. Payments for consumed heat T_1 and the fixed payment or the fee for installed capacity T_2 were estimated for all the 28 scenarios by applying equations (7) and (8) (Fig. 8).

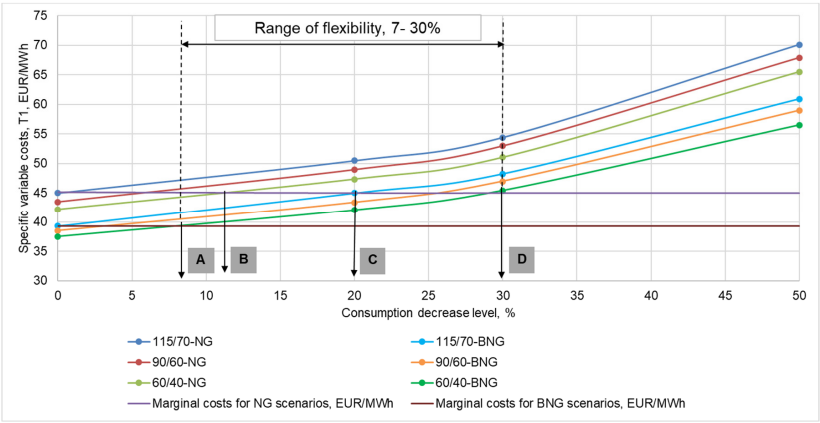

Fig. 8. Variable heat price by a two-part heat tariff.

In addition, the marginal costs per additional unit were calculated (9) (short-term marginal costs) for the DH system with the initial parameters (E-115/70-NG and E-115/70-BNG). The DH system is operated by natural gas in the initial situation and a high potential temperature schedule is maintained in the networks (115/70), the heat consumption reduction (improvement of energy efficiency at the customer's side) by 12 % will mean that even by transition to the lowest temperature schedule the utility will not be able to maintain the tariff at the preceding level (Fig. 8, point B). The DH systems where the aggregate fuel costs and variable costs are lower will be more sensitive to reduction of the heat consumption (Fig. 8, point A). Relatively more freedom in terms of reduction of heat consumption is provided to DH utilities

by the possibility of transition not only to the cheapest fuel (the consumption decrease of up to 20 % may not change the heat rate, see Fig. 8, point C), but also to a lower potential heat carrier (the consumption decrease of up to 30 % may not change the heat tariff, see Fig. 8, point D). Implementation of both conditions (low-temperature heat networks and renewable energy sources) corresponds to the definition of the 4th generation system and it is a sustainable solution.

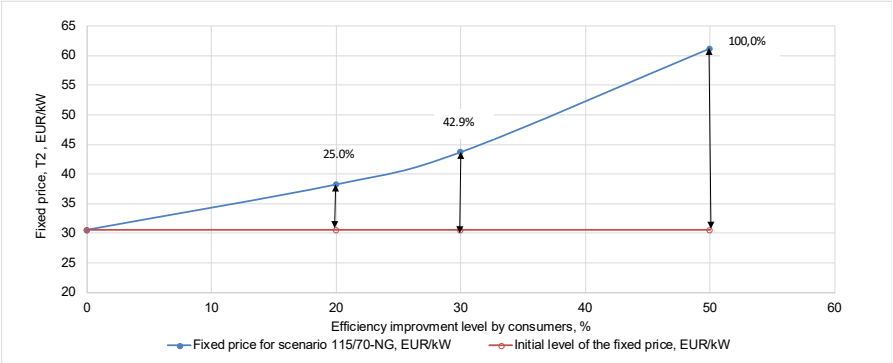

Fig. 9. Fixed price component for 115/70-NG scenario by changing the efficiency level at the consumer's side.

The second element of a two-part tariff is a fixed fee (it is also referred to as the capacity fee), which provides for maintenance of the installed generating capacity in the operational order for the DH utility. The fixed fee is the fee for capacity needed for ensuring heating of a property. Consequently, these are fixed payments to be paid by consumers irrespective of whether heat is or is not consumed. In order to make this fee comprehensible to customers, it is usually recalculated from EUR per installed capacity in kW or MW to EUR per square metre of heated floor area. In this way, the index clearly defines fixed fees payable by households. As the efficiency at the consumer's side increases by more than 20 %, the fixed fee increases rapidly according to a non-linear pattern (Fig. 9). Zvingilaite & Jacobsen [38] in their study concluded that improvement of efficiency at the consumer's side by 18.3 to 23.8 % is economically justified. The heat supply utility should find ways for compensating reduction of consumption. The DH system expansion is usually among the development scenarios implemented most often. However, transition to the 4th generation system forces DH utilities to look for other potential innovative solutions that comply with the circular economy principles and are sustainable accordingly. For example, JSC "Fortum" integrated production of biooil in the CHP plant operation in Joensuu (JSC Fortum, Joensuu CHP plant).

4.2.3. Introduction of the Consumption Quality Component in the Heat Pricing Methodology

Costs of heat production depend on numerous parameters. The volume of consumed heat is determined by using the system of equations presented in the methodology section (10) where the consumption of heat carrier G [m3/h] may be reduced by increasing the temperature difference between supply and return upon the condition that remains unchanged:

$$Q_{con} = G \downarrow c\Delta t \uparrow. \quad (10)$$

Thus, in order for the DH to be operated as efficiently as possible, it is important that there is a large temperature difference between the DH water that the property receives and the one sent back. The temperature difference is called cooling. DH companies in the deregulated market introduce the cooling requirement (for example, Δt=30 °C). If the cooling in the property is up to 5 °C higher or lower than the cooling requirement, no extra payment or bonus is charged. If the cooling over the year averages over 36 °C, a bonus is paid out.

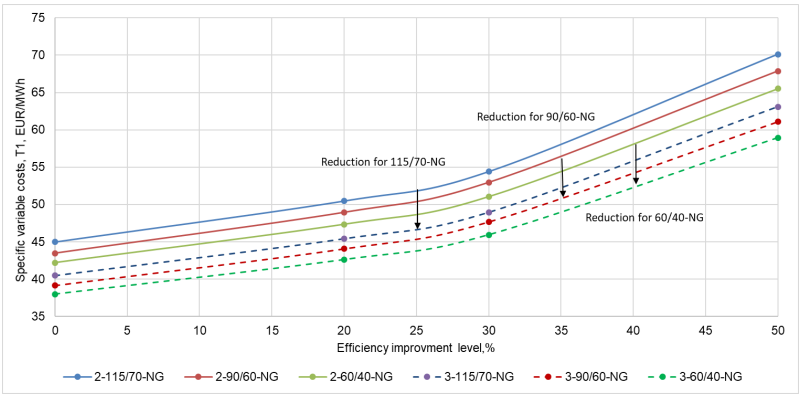

Fig. 10. Reduction in energy price T1 by qualitative heat carrier cooling at the consumer's side (115/70, 90/60 and 60/40 – the temperature regime in the DH network, NG – natural gas, 2 – a two-part heat tariff, 3 – a two-part heat tariff with additional quality component).

For instance, Fig.10 presents an adjusted energy component for the scenarios with a two-part tariff where natural gas is used as fuel. The adjustment level on the deregulated market is set by each DH utility independently according to the principle of economic profitability because generally reduction of the return temperature allows increasing the heat and electricity production efficiency. Efficiency of the 10MW condensation economiser is illustrated in Fig. 11.

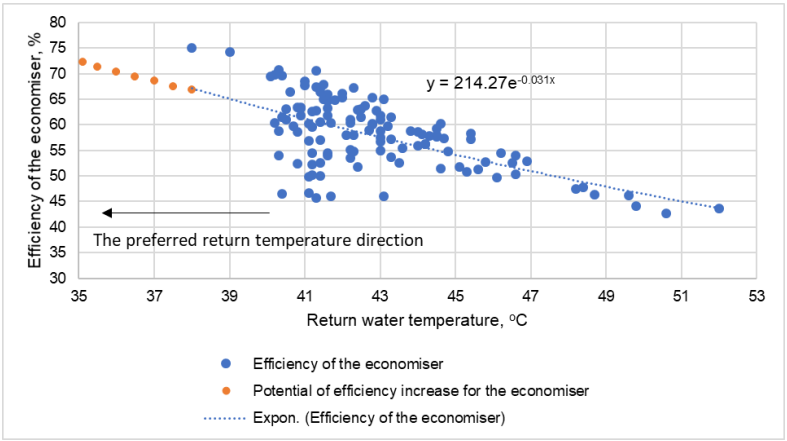

Fig. 11. Modelling of efficiency of the condensing unit versus network return temperature.

Modelling of efficiency of the condensation economiser (orange dots) clearly shows that the productivity of the economiser increases as the return temperature decreases. However, reduction of the return temperature may be provided only by the consumer by means of intensifying the heat exchange processes or by increasing the heat exchange surfaces through installing heat exchangers and heating elements. Reduction of the return temperature, which will also allow increasing the temperature difference, also secures other advantages related to the overall efficiency of the DH systems (Fig. 12).

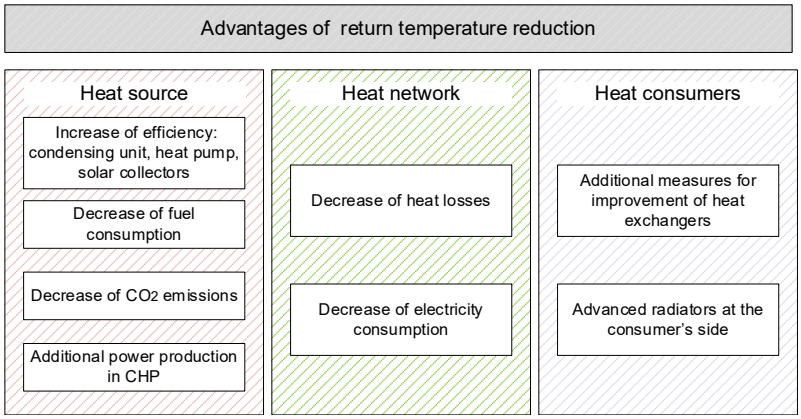

Fig. 12. Advantages of the reduction of return temperature in the DH network.

Efficiency is improving not only in condensing economisers, but also the operation of solar collectors and heat pumps is getting more efficient, the CHP productivity increases. The total DH system efficiency improvement allows reducing expenses and offering the lowest heat tariff, which is emphasised by A. Dalla Rosa et. al in their study [39]. Considering the fact that high-level professionals, who carefully follow up innovations in the heat supply area and perform energy efficiency measures, manage the DH utility, this generally allows reducing energy production costs and providing more optimum heat tariffs to customers.

5. CONCLUSIONS

Transition to the 4GDH systems causes new challenges for DH utilities regarding implementation of innovative technologies characterised by low-temperature heat sources, low-temperature transmission networks and low consumption buildings within a common smart energy system. Heat pricing is an essential issue to be taken into account by trying to achieve sustainable development of DH systems setting new tasks for all the parties involved in the DH system (DH utilities, consumers, property developers, policy makers and other stakeholders). The study reveals that the current procedure when consumers pay to DH utilities on a regulated market based on the one-part tariff has to be changed because transition to the 4th generation systems is related to the improvement of energy efficiency at the customer's side, reduction in the temperature schedule and implementation of an open network (provision of the third party access).

The study has demonstrated that DH utilities have to follow up carefully changes in heat consumption. Transition to a lower temperature schedule and use of cheaper fuel allows implementing energy efficiency measures within the framework of 20–30 % without changing the tariff.

The study has confirmed that implementation of the two-part tariff will allow DH utilities to compensate fixed costs incurred by maintaining the heat generating plant in the good operational condition. Consumers, however, will need to assess the demanded capacity carefully. In order to encourage consumers to improve efficiency of heat exchangers and heating elements by implementing modernisation measures, it is necessary to introduce the energy quality component (temperature difference between supply and return temperature). The energy quality component will allow reducing payments for the consumers who have improved their heat supply systems, and consumers who have low efficiency systems will have to pay more.

The methodology proposed in the present article allows evaluating the tariff changes and their development trends within the transition from the current DH system to the 4GDH system by maintaining its competitiveness. The optimum solution for the DH system development in order to follow the direction towards the 4GDH system prescribes that the best design should reduce the utility costs and, more importantly, provide an optimum heat price for end customers. Therefore, A DH company policy should base on the three pillars of sustainability - economic feasibility, high-level environmental performance and social responsibility strategy.

REFERENCES

1. Lund, H., Werner, S., Wiltshire, R., Svendsen, S., Thorsen, J., Hvelplund, F., & Mathiesen, B.V. (2014). 4th generation district heating (4GDH) integrating smart thermal grids into future sustainable energy systems. *Energy, 68*, 1–11, DOI: 10.1016/j.energy.2014.02.089.
2. Pieper, H., Ommen, T., Elmegaard, B., & Markussen, W.B. (2019). Assessment of a combination of three heat sources for heat pumps to supply district heating. *Energy, 176*, 156–170, DOI: 10.1016/j.energy.2019.03.165.
3. Hammer, A., Sejkora, C., & Kienberger, T. (2018). Increasing district heating networks efficiency by means of temperature-flexible operation. *Sustainable Energy, Grids and Networks, 16*, 393–404, DOI: 10.1016/j.segan.2018.11.001.
4. Werner, S. (2017). International review of district heating and cooling. *Energy*, *137,* 617–631, DOI: 10.1016/j.energy.2017.04.045.
5. European Commission (2008). 3 Communication from the Commission to European Parliament, the Council, the European Economic and Social Committee and the Committee of the Regions – 20 20 by 2020: Europe's climate change opportunity. *European Commission,COM(2008),30 Final*, 1–12.
6. Eurostat (n.d.). Available at: http://ec.europa.eu/eurostat/statistics-explained/index.php/Energyconsumption_in_households#cite_note-1.
7. Lund, H., Østergaard, P., Connolly, D., & Mathiesen, B.V. (2017). Smart energy and smart energy systems. *Energy*, 1–10, DOI: 10.1016/j.energy.2017.05.123.
8. European Parlament (2009). Directive 2009/72/EC of the European Parliament and of the Council of 13 July 2009 concerning common rules for the internal market in electricity and repealing Directive 2003/54/EC. *Official Journal of the European Union, L 211/55*, 55–93.

9. European Comission (2016). An EU Strategy on Heating and Cooling. *Communication from the Commission to the European Parliament, the Council, the European Economic and Social Committee and the Committee of the Regions, COM(2016), 51 Final*, 1–13.
10. Eurostat (2018). Energy balance sheets. 2016 data. *Eurostat*, 1–116.
11. Rehman, H., Hirvonen, J., & Sirén, K. (2018). Performance comparison between optimized design of a centralized and semi-decentralized community size solar district heating system. *Applied Energy, 229*, 1072–1094, DOI: 10.1016/j.apenergy.2018.08.064.
12. Renaldi, R., & Friedrich, D. (2019). Techno-economic analysis of a solar district heating system with seasonal thermal storage in the UK. *Energy Policy, 236*, 388–400, DOI: 10.1016/j.apenergy.2018.11.030.
13. Pacot, P., & Reuter, S. (2011). Quality indicators for district heating networks. Available at: http://hdl.handle.net/2268/96467.
14. Iddrisu I., & Bhattacharyya, S. (2015). Sustainable energy development index: A multi-dimensional indicator for measuring sustainable energy development. *Renewable and Sustainable Energy Reviews, 50*, 513–530, DOI: 10.1016/j.rser.2015.05.032.
15. Romanchenko, D., Odenberger, M., Göransson, L., & Johnsson F. (2017). Impact of electricity price fluctuations on the operation of district heating systems: A case study of district heating in Göteborg, Sweden. *Applied Energy, 204*, 16–30, DOI: 10.1016/j.apenergy.2017.06.092.
16. Ziemele, J., Vigants, G., Vitolins, V., Blumberga, D., & Veidenbergs, I. (2014A). District heating systems performance analyses. heat energy tariff. *Environmental and Climate Technologies, 13*, 32–43, DOI: 10.2478/rtuect-2014-0005.
17. Büchele, R., Kranzl, L., & Hummel, M. (2018). What is the impact of the policy framework on the future of district heating in Eastern European countries? The case of Brasov. *Energy Strategy Reviews, 19*, 72–75, DOI: 10.1016/j.esr.2017.12.003.
18. Koirala, B., Koliou, E., Friege, J., Hakvoort, R., & Herder, P. (2016). Energetic communities for community energy: A review of key issues and trends shaping integrated community energy systems. *Renewable and Sustainable Energy Reviews, 56*, 722–744, DOI: 10.1016/j.rser.2015.11.080.
19. Hansen, C., Gudmundsson, O., & Detlefsen, N. (2019). Cost efficiency of district heating for low energy buildings of the future. *Energy, 177*, 77–86, DOI: 10.1016/j.energy.2019.04.046.
20. Turski, M., & Sekret, R., (2018). Buildings and a district heating network as thermal energy storages in the district heating system. *Energy & Buildings, 179*, 49–56, doi.org/10.1016/j.enbuild.2018.09.015.
21. Zhang, J., Ge, B., & Xu, H. (2013). An equivalent marginal cost-pricing model for the district heating market. *Energy Policy, 63*, 1224–1232, DOI: 10.1016/j.enpol.2013.09.017.
22. Public Utilities Commission of Latvia (2010). *Methodology for the Calculation of Thermal Energy Supply Service Tariffs*. Decision No. 1/7 of the Board of the Public Utilities Commission.
23. Central Statistical Bureau (2019). Available at: http://data1.csb.gov.lv/pxweb/lv/vide/vide__energetika__ikgad/?tablelist=true
24. Tol, H.I., & Svendsen, S. (2015). Effects of boosting the supply temperature on pipe dimensions of low-energy district heating networks: A case study in Gladsaxe, Danmark. *Energy and Buildings, 88*, 324–334, DOI: 10.1016/j.enbuild.2014.10.067.
25. Dalla Rosa, A., & Christensen, J. (2011). Low-energy district heating in energy-efficient building areas. *Energy, 36*, 6890–6899, DOI: 10.1016/j.energy.2011.10.001.

26. Cai, H., You, S., Wang, J., Bindner, H.W., & Klyapovskiy, S. (2018). Technical assessment of electric heat boosters in low-temperature district heating based on combined heat and power analysis. *Energy*, *150*, 938–949, DOI: 10.1016/j.energy.2018.02.084.
27. Dalla Rosa, A., Li, H., Svendsen, S., Werner, S., Persson, U., Ruehling, K., & Felsman, C. (2014). *Toward 4th generation district heating: Experince and potential of low-temperature district heating.* Germany: International Energy Agency.
28. Averfalk, H., Werner, S., Felsmann, C., Rühling, K., Wiltshire, R., & Svendsen, S. (2017). *Transformation roadmap from high to low temperature district heating systems. Annex XI final report.* International Energy Agency.
29. Li, H., & Wang, S.J. (2014). Challenges in smart low-temperature district heating development. *Energy Procedia, 61*, 1472–1475, DOI: 10.1016/j.egypro.2014.12.150.
30. Okkonen, L., & Suhonen, N. (2010). Business models of heat entrepreneurship in Finland. *Energy Policy, 38*, 3443–3452, DOI: 10.1016/j.enpol.2010.02.018.
31. Prando, D., Renzi, M., Gasparella, M., Gasparella, A., & Baratieri, M. (2015). Monitoring of the energy performance of a district heating CHP plant based on biomass boiler and ORC generator. *Applied Thermal Engineering, 79*, 98–107, DOI: 10.1016/j.applthermaleng.2014.12.063.
32. Madlener, R. (2007). Innovation diffusion, public policy, and local initiative: The case of wood-fuelled district heating systems in Austria. *Energy Policy, 35*, 1992–2008. DOI: 10.1016/j.enpol.2006.06.010.
33. Ilic, D., & Trygg, L. (2014). Economic and environmental benefits of converting industrial processes to district heating. *Energy Conversion and Management, 87*, 305–317, DOI: 10.1016/j.enconman.2014.07.025.
34. Paiho, S., & Saastamoinen, H. (2018). How to develop district heating in Finland? *Energy Policy, 122*, 668–676, DOI: 10.1016/j.enpol.2018.08.025.
35. Sarma, U., & Bazbauers, G. (2016). District heating regulation: parameters for the benchmarking model. *Energy Procedia, 95*, 401–407, DOI: 10.1016/j.egypro.2016.09.046.
36. Li, H., Sun, Q., Zhang, Q., & Wallin, F. (2015). A review of the pricing mechanisms for district heating systems. *Renewable and Sustainable Energy Reviews, 42*, 56–65, DOI: 10.1016/j.rser.2014.10.003.
37. Köfinger, M., Basciotti, D., Schmidt, R., Meissner, E., Doczekal, C., & Giovannini, A. (2016). Low temperature district heating in Austria: Energetic, ecologic and economic comparison of four case studies. *Energy, 110*, 95–104, DOI: 10.1016/j.energy.2015.12.103.
38. Zvingilaite, E., & Klinge Jacobsen, H. (2015). Heat savings and generation technologies:Modelling of residential investment behaviou with local health costs. *Energy Policy, 77*, 31–45, DOI: 10.1016/j.enpol.2014.11.032.
39. Dalla Rosa, A., Boulter, R., Church, K., & Svendsen, S. (2012). District heating (DH) network design and operation toward a system-wide methodology for optimizing renewable energy solution (SMORES) in Canada: A case study. *Energy, 45*, 960–974, DOI: 10.1016/j.energy.2012.06.062.

IZAICINĀJUMI UN BARJERAS PĀREJAI UZ 4. PAAUDZES CENTRALIZĒTĀS SILTUMAAPGĀDES SISTĒMU. CENU MEHĀNISMA VEIDOŠANAS STRATĒĢIJA

U. Osis, N. Talcis, J. Ziemele

K o p s a v i l k u m s

Centralizētās siltumapgādes pāreja uz 4.paaudzes sistēmu saistīta ar vairākiem izaicinājumiem, kas paredz ne tikai inovatīvo tehnoloģiju ieviešanu, bet saistīti arī ar ilgtspējīga tarifa aprēķina metodoloģijas izstrādāšanu. 4.paaudzes sistēmu ieviešana jau tuvākajā laikā liks siltumapgādes nozarei rast atbildes par iespēju organizēt siltumapgādi līdzīgi kā tas notika elektroenerģijas nozarē (Directive 2009/72/EC), pilnīgi nodalot ražotājus no pārvades sistēmas pakalpojumu sniedzējiem. Rakstā pētīti dažādi siltumapgādes uzņēmuma attīstības scenāriji regulētā pakalpojuma ietvaros un to tarifu noteikšanas metodikas, ka arī vērtēta to ilgtspējība, ņemot vērā pāreju uz 4.paaudzes sistēmām.

17.07.2019.

sciendo

LATVIAN JOURNAL OF PHYSICS
AND TECHNICAL SCIENCES
2019, N 4

DOI: 10.2478/lpts-2019-0023

OPTIMISATION OF PERMANENT MAGNETS OF BIOREACTOR MAGNETIC COUPLING WHILE PRESERVING THEIR EFFICIENCY

M.Konuhova[1], E.Kamolins[1,2], S.Orlova[1], A.Suleiko[3], R.Otankis[1]

[1]Institute of Physical Energetics,
11 Krivu Str., Riga, LV-1006, LATVIA
e-mail: mkonuhova@gmail.com
[2]Riga Technical University
12/1 Azenes Str., Riga, LV-1048, LATVIA
[3]Latvian State Institute of Wood Chemistry
27 Dzerbenes Str., Riga, LV-1006, LATVIA

The paper discusses issues related to the optimisation of magnetic couplings used in bioreactors (manufactured by JSC "Biotehniskais Centrs"). The purpose of optimisation was to preserve the maximum breakaway torque of the magnetic coupling while reducing the mass of rare earth elements used in its structure. The paper presents the rationale for the selected optimisation option taking into account the economic aspect. To solve the optimisation problem, the factors affecting the maximum torque of the magnetic coupling, such as the shape and height of the internal and external magnets, the angle of the external and internal magnets, as well as the height of the internal and external yoke, were determined. The design of the existing magnetic coupling was optimised and its prototype was made based on the results of optimisation. The results obtained by means of optimisation were compared with the results obtained experimentally by testing the manufactured prototype.

Keywords: *bioreactors, design optimisation, industrial application, magnetic device, modelling, test bench*

1. INTRODUCTION

European manufacturers of biotechnological equipment are increasingly using mixers with magnetic coupling. Bioreactors are used in biotechnological processes aimed at producing biopharmaceuticals. Many medical drugs obtained this way contribute to an increase in the expectancy of healthy life. Moreover, it should be noted that many of these drugs can only be obtained using biotechnological methods. Biotechnological processes for the production of these drugs usually meet the requirements of good manufacturing practice (GMP). In this case, the magnetic coupling is used in bioreactors to ensure sterile mixing of nutrient media [1], [2]. In

addition to ensuring sterility, the mixers must provide high performance, i.e. having a sufficient maximum torque, which is ensuring the necessary mixing intensity. Therefore, designing high performance equipment is a relevant objective at the moment.

Magnetic couplings (MC) with permanent magnets are known to be able to transmit torque through the magnetic forces between the internal and external rotors (Fig. 1). In this type of MC its driving and driven parts are hermetically separated. At the same time, the transmission of vibration torque is very low due to the lack of mechanical feedback [3]. Magnetic coupling has one particularly valuable feature: it can operate with classical types of electric motors, while the motor is placed outside the operation area of the coupling. The application of magnetic couplings is continuously expanding; this is facilitated by the production of up-to-date permanent magnets (PM) based on rare earth elements. Magnetic couplings have one more important feature: they protect the mechanism from overload, as in case of operational overload of the driven part, magnetic connection between the rotors is terminated and the motor does not go into short-circuit fault mode.

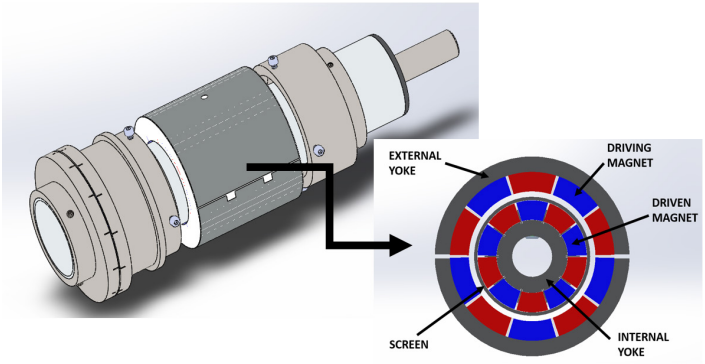

Fig. 1. Magnetic coupling of a bioreactor.

JSC "Biotehniskais Centrs" produces magnetic couplings for bioreactors of different volumes (5 dm^3, $1m^3$, $4m^3$, 15 m^3, etc.). In this paper, we review in detail the design of the magnetic coupling for $1m^3$ bioreactor with an average diameter of the air gap $D_{\delta\,avg} = 60$ mm.

2. INITIAL BIOREACTOR MAGNETIC COUPLING

The bioreactor magnetic coupling with an average diameter of the air gap $D_{\delta\,avg.} = 60$ mm has the following design parameters:

- External radius, $R_1 = 40.5$ mm;
- Air gap, $\delta = 4.11$ mm – 4.76 mm;
- PM type – N48H ($t_{max} = 120°C$);
- PM axial length, $l = 3x25.4 = 76.2$ mm;
- Internal and external PM height, $h_{PM} = 6.35$ mm;
- Internal and external PM width, $b_{PM} = 12.7$ mm;

- Number of pole pair, $p = 5$;
- PM manufacturer – *K&J* magnetics;
- PM remanence, $B_r = 1.36$ T;
- PM coercivity, $H_c = 907\ 183$ kA/m.

The initial dimensions of the magnetic coupling are shown in Fig. 2a. As it can be seen from Fig. 2, the coupling has 10 magnets placed on the inner yoke and 10 magnets placed on the outer yoke. All magnets are made on the basis of rare earth elements NdFeB (N48H magnets) and have the same size and rectangular shape. Magnetization of magnets of this shape is linear and is carried out throughout the whole thickness (T) of the magnet (Fig. 2b). The air gap in the design varies between 4.11 mm ÷ 4.76 mm, depending on the rotation of the internal rotor relative to the external one.

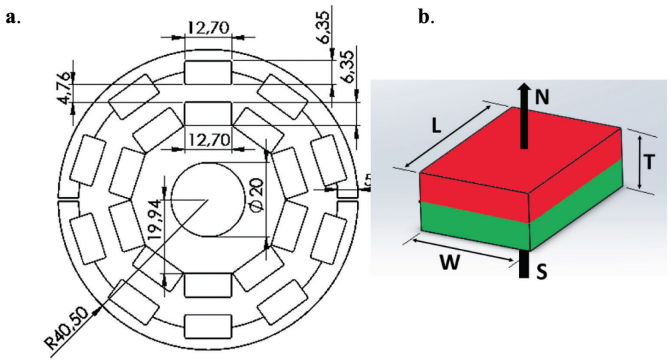

Fig. 2. a) Cross-section of magnetic coupling with rectangular magnets; b) Direction of magnetization of rectangular magnets (T- thickness, W-width, L-length, N-north pole, S-south pole).

Magnetic field of the coupling when the internal rotor is rotated to an angle $\theta = 0°$ and an angle $\theta = 18°$ is depicted in Fig. 3. The θ angle is the angle of shift between the inner and outer rotors. The angle $\theta = 18°$ is the rotation angle at which the magnetic coupling torque is at the maximum, and the angle $\theta = 0°$ corresponds to the minimum value of the torque.

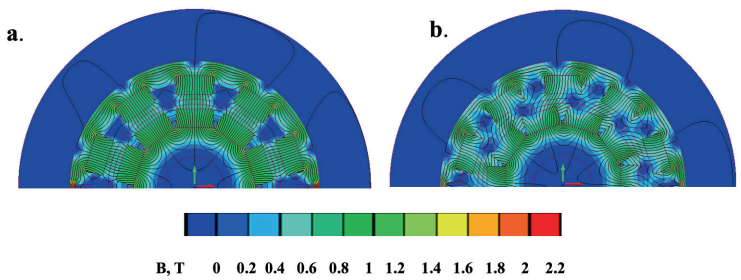

Fig. 3. Magnetic field of the coupling with rectangular magnets: a) $\theta = 0°$; b) $\theta = 18°$.

According to the results of numerical modelling based on the finite element method (FEM), the maximum torque of MC is $M_{\max\_mod} = 50.2\ Nm$, and the maximum experimentally obtained torque is $M_{\max\_exp} = 49.075\ Nm$.

The specific torque of permanent magnets is calculated by the equation:

$$M_{spec.t._NdFeB} = \frac{M_{\max}\left[N \cdot m\right]}{G_{NdFeB\_total}\left[kg\right]} = \left[N \cdot m/kg\right], \quad (1)$$

where $M_{\max}$ – maximum torque of MC, *Nm*;

G_{NdFeB_total} – total magnet mass, kg.

There are many factors affecting the maximum torque (Fig. 4).

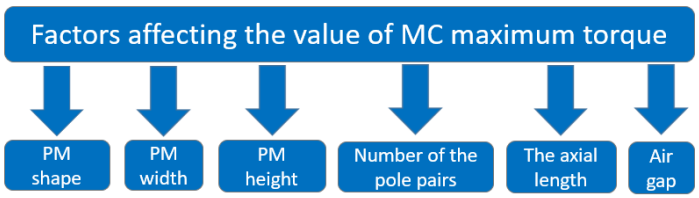

Fig. 4. Factors affecting the value of magnetic coupling maximum torque.

All of these factors affecting the maximum torque were taken into account in optimisation of the magnetic coupling design. However, it should be noted that when optimising the design focused on an increase in the maximum torque, an increase in the mass of magnets cannot be avoided, and this in turn will lead to a rise in the cost of production [4]. In this regard, the main optimisation objective was to preserve the value of the coupling maximum torque, while reducing the volume of rare earth elements (permanent magnets) in the design. The rationale for this optimisation solution is presented in Section 3.

3. SELECTION OF OPTIMISATION METHOD AND ITS RATIONALE

Rare earth elements such as neodymium and dysprosium are used in NdFeB magnet structure. However, the supply of these elements mainly depends on China. In 2018, according to statistical estimates, the world reserves were 120 million tons, most of which were located in China, i.e. about 44 million tons (Fig. 5).

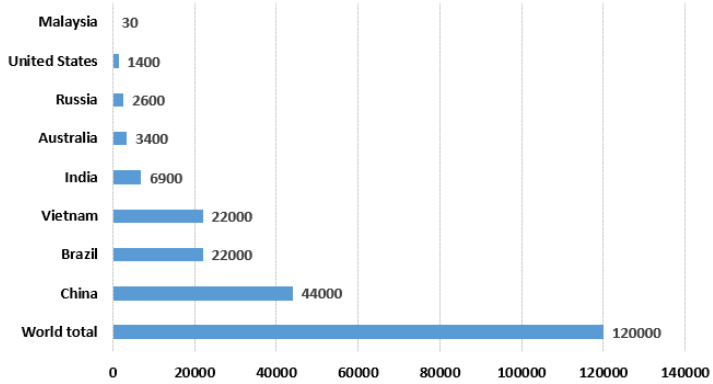

Fig. 5. Rare earth reserves worldwide as of 2018, by country (in thousand tons).

How much the world depends on Chinese rare earth elements became clear at the end of 2010, when China threatened to limit the supplies. The price increase of rare earth elements was very significant, for example, the cost of neodymium and dysprosium increased about 25 times. Prices for most of the elements have declined significantly since 2012, but there is a big doubt about the future availability and price of rare earth magnets. Many experts anticipate supply shortage of some rare earth metals in the future, as demand is expected to exceed the industry's capacity to produce these rare earth elements over time. It is expected that the price of neodymium will reach about 104 549 USD per ton in 2020, and in 2025 it is expected that the price will grow up to more than 148 thousand USD per ton [5].

Even such global scale manufacturers as Tesla, Inc. are concerned about the current situation regarding the rise in prices for rare earth elements, which may affect the price of production of electric vehicles [6].

Therefore, in this context, the main objective is to optimise the magnetic coupling in order to reduce the volume of rare earth elements for the production of magnetic couplings, while maintaining its maximum torque, since the rejection of permanent magnets is not possible.

Considering the above-mentioned facts, the purpose of optimisation was related to the economic effect.

4. OPTIMISATION AND ITS RESULTS

Many analysis models for electrical machines are based on FEM instead of the analytical model and equivalent circuit model. Therefore, intelligent optimisation algorithms have been employed for the optimisation of electrical machines in the past several decades, such as the evolutionary algorithms (EAs), particle swarm optimisation (PSO) algorithms, estimation of distribution algorithms (EDAs), immune algorithms, and ant colony algorithms, and their improvements. For the widely used genetic algorithm (GA) and differential evolutional algorithm (DEA), they are two of four major subclasses of EAs. The other two subclasses are evolution programming and evolution strategy [7].

For MC optimisation Mentor (A Siemens Business) software OptiNet in conjunction with MagNet was applied. To solve the optimisation problem, an evolutionary algorithm had been selected. It is obvious that the classical approach has a large number of algorithms and is constantly being developed by mathematicians; however, these algorithms usually give one solution.

Optimisation using a genetic algorithm results in obtaining a set of solutions with the best one being selected. The evolutionary algorithm preserves the population of solutions throughout the optimisation process; therefore, many solutions are obtained at the end of the optimisation process. For the multi-criteria optimisation, it is better to obtain a set of solutions instead of one, and as a result, evolutionary algorithm is a more useful approach [8].

To optimise the magnetic coupling, the following parameters have been selected: height of the inner yoke (h_{int_j}), height of the outer yoke (h_{ext_j}), height of internal and external magnets (h_{int_PM}, h_{ext_PM}), angle of internal and external magnets

(α_{PM}), while the average diameter of the air gap remained unchanged $D_{\delta\,avg}$ = 60 mm.

As a result of the optimisation of the magnetic coupling, the transition from the rectangular shape of the magnets to the arc-shaped was carried out, thereby ensuring the uniformity of the air gap, the height of the internal and external magnets was significantly reduced, and the height of the internal and external yoke obtained its optimal value.

The optimisation results are presented in Table 1, which also shows the parameters of the initial coupling and the results of comparing the initial design and the coupling structure after optimisation.

Table 1

Summary of 1 m3 Bioreactor Magnetic Coupling Optimisation Results

Parameters	Initial (numerical modelling)	After optimisation (numerical modelling)	Comparison
External radius, mm	40.5	44.23	+9.2 %
Coupling axial length, mm	76.2	76.2	
Air gap, mm	4.11 – 4.76	4.11	
PM type	N48H (t_{max} = 120°C)	N48H	
PM axial length, mm	3x25.4 = 76.2	3x25.4 = 76.2	
External PM height, mm	6.35	4.44	-43 %
Internal PM height, mm	6.35	4.4	-44 %
External PM width, mm	12.7		
Internal PM width, mm	12.7		
Internal PM angle, deg	-	31	
External PM angle, deg	-	34.56	
Number of pole pairs	5	5	
PM manufacture	K&J magnetics	K&J magnetics	
PM remanence, T	1.36	1.36	
PM coercivity, kA/m	907 183	907 183	
PM density, kg/m^3	7500	7500	
PM total mass, kg	0.919	0.844	-8.88 %
Maximum torque M_{max}, Nm	50.2	56.07	+11.69 %
PM specific torque, Nm/kg	54.6	66.43	+21.66 %

Coupling design and size are presented in Fig. 6.

Images of the magnetic field of the optimised magnetic coupling when the internal rotor is rotated by an angle of $\theta = 0°$ (minimum torque value) and an angle of $\theta = 17°$ (maximum torque value) are presented in Fig. 7.

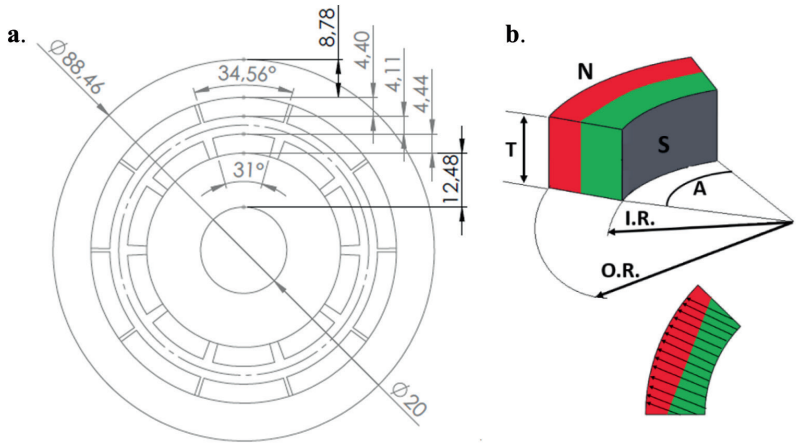

Fig. 6. a) Cross-section of magnetic coupling with arc-shaped magnets after optimization; b) Magnetization of arc-shaped K&J magnets (T- thickness, A-angle, I.R.-inner radius, O.R.-outer radius, N-north pole, S-south pole).

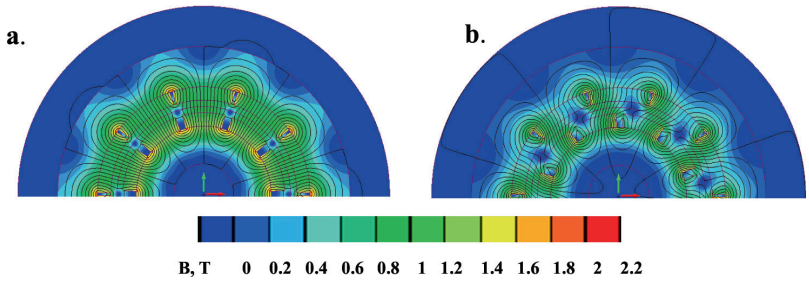

Fig. 7. Magnetic field of a coupling with arc-shaped magnets a) $\theta = 0°$; b) $\theta = 17°$.

As a result of the design optimisation, the value of the maximum torque of the initial coupling was increased by 11.69 % according to the results of numerical modelling, and the consumption of PM was reduced by 8.88 %. At the same time, the specific torque of the magnets increased by 21.66 %, according to the results of numerical modelling.

5. EXPERIMENTAL STUDY

A prototype magnetic coupling of 1 m^3 bioreactor with the arc-shaped magnets with an average diameter of the air gap $D_{\delta\,avg}$ = 60 mm that was constructed according to the optimisation result was tested in the study. Experimental studies of the prototype made it possible to verify the results obtained by numerical modelling. During the study, the maximum torque at which the "breakdown" of the magnetic coupling occurred was determined. The test bench is presented in Fig. 8. The test bench consists of an electric motor (U_{MAX} - 60 V, n_{MAX} - 3350 rpm) and a magnetic coupling. The operating voltage of motor is 24V, which corresponds to the MC

rotational speed of 200 rpm. The measurements were made using a mass sensor (CAS, BCS-60BW), with the measurement range of 0 kg – 60 kg and measurement accuracy of ± 0.005 kg.

The inner rotor is turned by an angle measured with voltage sensor that is placed on the inner rotor and connected with oscilloscope. After fixing the turning angle, the interaction forces between the PMs on both rotors try to turn the outer rotor on which the support system 1 is mounted. When the outer rotor tries to rotate (white arrow), the pressure force F is made by the arm of force l = 200 mm and measured by the sensor 2 (Fig. 8).

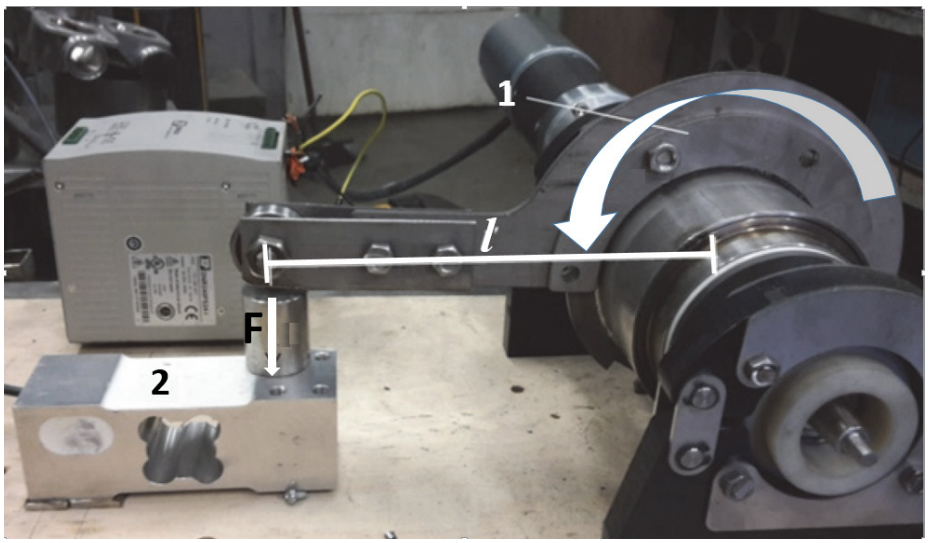

Fig. 8. Test bench.

The mechanical torque during the experiments was calculated from the mass readings as follows:

$$T = m \cdot l \cdot g\,, \tag{2}$$

where T – the mechanical torque generated on the mixers shaft, m – the mass reading from the load cell, l – the length of stainless steel rod, g – constant of gravitational acceleration.

Table 2

The Results of Experimental Study

Parameter	1 m^3
Maximum torque, Nm (experiment)	49.69

6. COMPARISON OF NUMERICAL MODELLING RESULTS AND OPTIMISATION RESULTS

Table 3 presents the values of the maximum and specific torque obtained theoretically and experimentally for the initial MC with rectangular magnets and the values of the maximum and specific torque of the new prototype with arc-shaped magnets.

Table 3

Comparison of Numerical Modelling and Experimental Data

Parameters	Initial MC	Optimised MC	Comparison
$M_{max\_mat.model.}$, Nm	50.2	56.07	+11.69 %
$M_{max\_exper.}$, Nm	49.075	49.69	+1.81 %
$M_{specific\_mat.model.}$ Nm	54.6	66.43	+21.66 %
$M_{specific\_experim.}$ Nm	53.40	58.87	+10.25 %

The results obtained theoretically differ from the results obtained experimentally, which is explained by the features of actual assembled unit, as well as the error range of the measuring instruments. It should be noted that in the modelling all the parameters of the raw materials were obtained from the documentation provided by the supplier (manufacturer), without any additional assumptions by the researchers.

The difference in the torque values between the experimental study and numerical modelling can be explained by the fact that in actual K&J magnets, the magnetization goes along the straight axis and is not radial (as it is considered in numerical modelling), the lines converge in the centre of the arc (Fig. 6b).

The specific torque of initial MC permanent magnets was increased by 21.66 % being equal to $M_{spec.t.\_NdFeB} = 66.43Nm$.

However, in spite of the difference of maximum torque obtained by theoretical and experimental studies, the mass of the magnets decreased by 8.88 % in the new optimised MC, and the new coupling, according to the experimental data, increased the value of the maximum torque by 1.81 %.

7. CONCLUSIONS

The study has revealed that the use of software based on FEM in conjunction with optimisation provides good results that can be fully applied in practice. Initially, the optimisation objective of reducing the mass of magnets was successfully completed, with maximum MC torque increase by 1.81 %, although originally the objective was simply not to reduce the available maximum torque value. The decrease in the mass of magnets used in the design by 8.88 %, taking into account the current increase in prices on the market of rare-earth elements, is significant. This kind of optimisation, based on the evaluation algorithm, can be surely applied to other magnetic couplings that use rare earth elements.

As a recommendation, it can be noted that in the numerical modelling of magnetic couplings with arc-shaped magnets, it is possible to reduce the performance value of magnets by 5–10 %, which will bring the calculations to the actual figures, as magnetization of arc-shaped magnets occurs linearly, rather than along the arc-shape.

ACKNOWLEDGEMENTS

The research has been supported by the European Regional Development Fund within the project "Influence of the Magnetic Field Initiated Stirring on Biotechnological Processes" No. 1.1.1.1/16/A/144.

REFERENCES

1. Jagani, N., Jagani, H., Hebbar, K., Gang, S.S., Vasanth Raj, P., Chandrashekhar, R.H., & Rao, J. V. (2010). An overview of fermenter and the design considerations to enhance its productivity, *Pharmacologyonline*, *1*, 261–301.
2. Varley, J., & Birch, J. (1999). Reactor design for large scale suspension animal cell culture. *Cytotechnology, 29*, 177–205. doi:10.1023/A:1008008021481.
3. Li, Z., Wang, D., Zheng, D., & Yu, L. (2017). Analytical modeling and analysis of magnetic field and torque for novel axial flux eddy current couplers with PM excitation. *AIP Advanced, 7*, 105303.
4. Orlova, S., Kamolins, E., Konuhova, M., & Suleiko, A. (2018). Design of magnetic couplings for bioreactors: Analytical treatment and optimization. In: *IEEE 2018 20th European Conference on Power Electronics and Applications (EPE'18 ECCE Europe)*, 17–21 September 2018, Riga, Latvia.
5. Statista. (n.d.). *Rare earth reserves worldwide as of 2018, by country*. https://www.statista.com/statistics/277268/rare-earth-reserves-by-country/
6. Desai, P. (2018). Tesla's electric motor shift to spur demand for rare earth neodymium. *Reuters*. Available at: https://www.reuters.com/article/us-metals-autos-neodymium-analysis-idUSKCN1GO28I
7. Lei, G., Zhu, J., Guo, Y., Liu C., & Ma, B. (2017). A review of design optimization methods for electrical machines. *Energies 2017*, 10, 1962.
8. Besnerais, J.L., Lanfranchi, V., Hecquet, M., & Brochet, P. (2008). Multiobjective optimization of induction machines including mixed variables and noise minimization. *IEEE Transactions on Magnetics*, *44*(6), 1102–1105.

BIOREAKTORA MAGNĒTISKĀ SAJŪGA PASTĀVĪGO MAGNĒTU MASAS OPTIMIZĀCIJA, SAGLABĀJOT TĀS EFEKTIVITĀTI

M.Koņuhova, E.Kamoliņš, S.Orlova, A.Šuleiko, R. Otaņķis

K o p s a v i l k u m s

Šajā rakstā tiek aplūkoti jautājumi, kas saistīti ar bioreaktoros (JSC "Biotehniskais Centrs" production) izmantojamo magnētisko sajūga optimizēšanu. Optimizācijas mērķis bija saglabāt maksimālo magnētiskā sajūga "noraušanas" momentu, samazinot izmantojamo retzemju elementu (NdFeB) masu konstrukcijā. Rakstā aplūkots izvēlētā optimizācijas ceļa pamatojums, ņemot vērā ekonomisko aspektu. Lai veiktu optimizāciju, tika noteikti faktori, kas ietekmē magnētiskā sajūga maksimālo momentu, tādi kā: iekšējo un ārējo magnētu augstums un forma, iekšējo un ārējo magnētu leņķis, kā arī iekšējā un ārējā jūga augstums. Tika veikta esošā magnētiskā sajūga konstrukcijas optimizācija un, pamatojoties uz veiktās optimizācijas rezultātiem, izgatavots tās prototips. Optimizācijas ceļā iegūtie rezultāti tika salīdzināti ar rezultātiem, kas iegūti eksperimentālā ceļā, testējot izgatavoto prototipu.

15.07.2019.

sciendo

LATVIAN JOURNAL OF PHYSICS
AND TECHNICAL SCIENCES
2019, N 4

DOI: 10.2478/lpts-2019-0024

SOLID STATE PHYSICS

COMPUTER SIMULATIONS OF THE BAND STRUCTURE AND DENSITY OF STATES OF THE LINEAR CHAINS OF NaCl IONS

L.N. Myasnikova[1], A.S. Istlyaup[1], D.M. Sergeyev[1,2], N.N. Zhanturina[1], K.Sh. Shunkeyev[1], A.I. Popov[3]

[1]Zhubanov Aktobe Regional State University, 34 A.Moldagulova Ave., Aktobe, 030000, KAZAKHSTAN

[2]Begeldinov Military Institute of Air Defence Forces, 39 Moldagulova Ave., Aktobe, 030012, KAZAKHSTAN

[3] Institute of Solid State Physics, University of Latvia, 8 Ķengaraga Str., LV-1063 LATVIA

e-mail: myasnikova_ln@mail.ru, popov@latnet.lv

The paper presents the results of first-principles computer simulations of the band structure, the density of states, and the total energy of NaCl (NaCl, Na_2Cl_2, Na_3Cl_3, Na_4Cl_4, Na_6Cl_6) linear chains of atoms. Modelling of the specified characteristics is realised in the computer code Atomistix ToolKit combined with Virtual NanoLab. The total energy depends on the number of ions in the nanoobject under study, but practically does not depend on the geometric arrangement of ions.

Keywords*: NaCl, band structure, computer simulations, density of states, total energy*

1. INTRODUCTION

Alkali halides are the simplest and most representative ionic crystals. The alkali halides NaF, NaCl, NaBr, and NaI crystallize in the rock salt (B1) structure at ambient conditions. They have many interesting physical properties such as high melting point, strong miscibility, and large band gaps. Due to the fact that in these materials the effective exciton mechanism [1]–[10] of the formation of radiation defects is implemented, they are widely used as radiation detectors, such as scintillators [11]–[15] and a storage phosphors for image plate detectors and optically stimulated dosimeters [16]–[20]. Moreover, alkali halides are used as infrared (IR) optical windows and optoelectronic devices [21], [22].

Nowadays, the properties of alkali halide nanocrystals have attracted great

attention of experts in chemistry, physics, and engineering. Structural, electronic, dynamic, and chemical characteristics of materials depend primarily on the state (phase) and the degree (size) of aggregation. Atomic chains containing 3–500 particles exhibit unique physical and chemical phenomena, which are of both fundamental and technological significance, and provide ways and means to explore the "transition" from molecular to condensed-matter systems [23]. They are simultaneously regarded as fundamental objects, in which the molecular and solid properties are reflected [24]–[29]. There are three main areas of application: first, nanocrystalline structures represent the ultimate in miniaturization of solid-state materials. Second, many nanocrystal properties are dominated by their surfaces because a large fraction of the atoms lies in the outermost layer. Third, the finite size and number of atoms in a nanocrystal, which is often less than 10^3, mean that systems having the structures of bulk crystalline matter can be calculated with a precision typically reserved for atoms and molecules, using modern methods [30], [31].

In the last decade, many papers were published about the properties of alkali halide nanocrystals. They include results on the cohesion, bonding, and structures; crystallinity phenomena including cleaving and melting; molecular adsorption reactions; halide-transfer reactions; electron substitution, solvation, and spectroscopy; surface electron states; electronic excitations and photochemistry; multiple charging; and other subtle effects in nanolattices [23], [32]. However, some major issues remain open, such as the reliability of structural calculations, based on first-principles methods. With these calculations, most experimental results could be interpreted.

A deep understanding of the optical properties of solids is impossible without a detailed knowledge of their electronic structure. The electronic processes in ionic crystals are considered on the basis of the approximate quantum-mechanical theory where the motion of electrons and nuclei is separated based on adiabatic Born-Oppenheimer approximation [33], [34]. One of the characteristics of the reflecting property of a nano-objects is the electronic density of states: the number of allowed electron (or hole) states per volume for a given energy [31].

In this paper, an attempt was made to determine the band structure, the density of states, and the total energy of NaCl linear chains with different number of ions using the computer simulations of Atomistix ToolKit combined with Virtual NanoLab [35].

2. DESCRIPTION OF THE OBJECT AND METHODS OF RESEARCH

The isolated atoms of the alkali metal Na and the halogen Cl have the following electronic configuration: $Na^0 – 1s^2 2s^2 2p^6 3s^1$, $Cl^0 – 1s^2 2s^2 2p^6 3s^2 3p^5$. In NaCl matrix, the ions of the corresponding elements assume the following electronic configuration – $Na^+ – 1s^2 2s^2 2p^6$, $Cl^- – 1s^2 2s^2 2p^6 3s^2 3p^6$. As a result, the valence electron located on the outer shell of Na^0 completely passes to Cl^0.

We divided the studied NaCl objects into three categories: one-dimensional, two-dimensional and three-dimensional. The dimensional NaCl built chain of 2, 4, 6 and 12, alternating between a Na^+ ions and Cl^-. Plane of 4, 6, 8 and 12 ions are

constructed in the two-dimensional NaCl. Three-dimensional NaCl consists of 8 and 12 ions. The distance between the centres of the nearest ions in NaCl is 2.82 Å [36].

In the adiabatic approximation, the solution of the Schrödinger equation shows that the states of an excess electron in a crystal with a periodic field are described by the Bloch wave functions [37]

$$u_k\left(\vec{r}\right)\exp\left\{-i\left(\frac{E}{h}t-\vec{k}\vec{r}\right)\right\},$$

where the function $u_k\left(\vec{r}\right)$ has the translational symmetry of the lattice, E – energy, $\vec{k}$ – wave vector. For a face-centered alkali halide crystal, the first Brillouin zone is a fourteen-tetrahedron in the form of a truncated octahedron; six faces have the form of squares, eight – the form of regular hexagons. The Γ-point lies in the centre of the first Brillouin zone (k =0), the X-point lies in the centre of the square plane, the L-point is at the centre of the hexagon. Along the [100] axis, the value of the wave vector varies from 0 to k_x, along the [111] direction from 0 to k_L. In all alkali halide crystals, the maximum of the valence band and the minimum of the conduction band are located in the centre of the Brillouin zone (Γ point). The upper hole zones are formed from the *p*-states of the halogen and have a negative dispersion typical of the *p*-bands. The bottom of the conduction band has an *s*-character, the effective mass of the electron is isotropic and has a value of the order of (0.5-1) m_0.

Computer modelling was carried out within the framework of the density functional theory (DFT) in the local density approximation [38].

3. RESULTS AND DISCUSSION

The calculated band structure of one-dimensional NaCl is shown in Fig. 1. The calculated band gap for a chain of two ions is 10.25 eV, of four ions – 11.4 eV, of six – 8.45 eV and of twelve – 10.46 eV. Note that in the first case, the energy minimum is observed at the Γ point of the Brillouin zone. The upper valence band in alkali halide crystals is associated with *p*-states of halogen. Function $E\left(k\right)$ has a maximum at the Γ-point. Due to the spin-orbit interaction for the *p*-hole at the Γ-point, the zone is split into two components. For the upper component, the orbital and spin moments of the *p*-hole are parallel and $j^+ = 3/2$. For the lower component, the orbital and spin moments are antiparallel and $j^+=1/2$. At the Γ-point, the upper component can degenerate. At the X- and L-points of the Brillouin zone, the valence band splits into three components. The lowest valence band occurs mainly from the *s*-orbit of Cl halogen, while the chlorine *p*-orbit is very weakly bound to the *p*-state of Na, as can be seen from the density of states (Fig. 2). In Fig. 2*a*, we observe two peaks responsible for *s*-orbits. The peak near -12 eV is connected with the halogen Cl, and the peak in the vicinity of zero energy is connected with Na. Figure 2*b* presents *p*-states of NaCl.

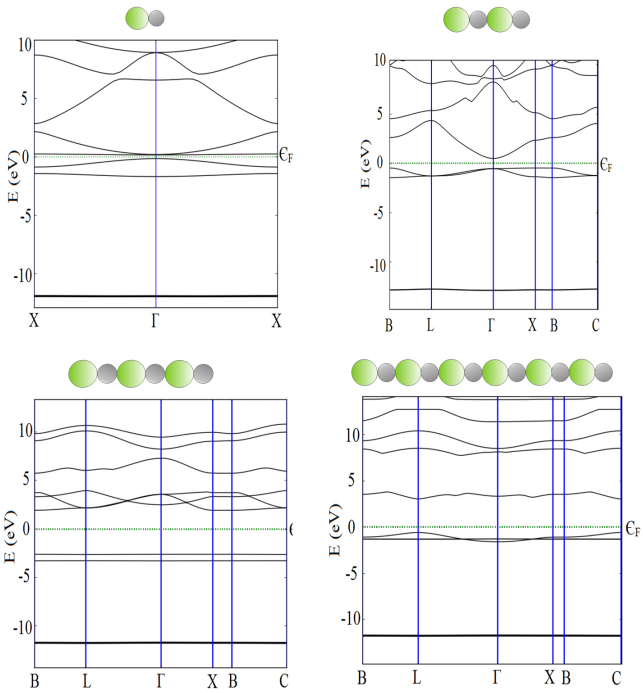

Fig. 1. Band structure of one-dimensional NaCl.
(Grey balls are sodium ions, green balls are chlorine ions)

The calculated band gap for NaCl, constructed on a plane of four ions, is 11.83 eV, of six – 11.46 eV, of eight – 11.55 eV and of twelve – 12.09 eV (Fig. 3). Note that the same for the bulk NaCl constructed from eight ions is 11.92 eV and from twelve to 11.12 eV (Fig. 3). Note that the experimental band gap energy for lowest-energy direct transition in crystalline NaCl was estimated to be 8.97±0.07 eV at 77°K [39].

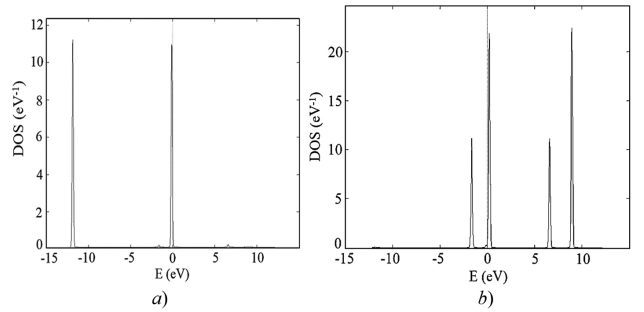

Fig. 2. Density of s (a), p (b) states of NaCl, consisting of one sodium ion and one chloride ion.

Table 1 shows the total energy of NaCl in 1-, 2- and 3- dimensions. We note that the value of the total energy depends on the number of ions in the object under study, but practically does not depend on the geometric arrangement of ions in space. At the same time, the values of the total energy vary in a narrow range, from -2815.15010 to -466.49970 eV. As we see from Table 1, with the increase in the

number of ions, the total energy decreases. For comparison, in Na_4Cl_3 cluster the total energy is higher to one order [31].

Table 1

Total and Specific Energy of NaCl

Object	Geometric location	Total energy, eV	Specific energy, eV
NaCl	1D	-466.49970	-233.24985
Na_2Cl_2	2D	-934.20591	-233.55148
Na_2Cl_2	1D	-934.68737	-233.67184
Na_3Cl_3	2D	-1398.40833	-233.06806
Na_3Cl_3	1D	-1398.79007	-233.13117
Na_4Cl_4	2D	-1864.85786	-233.10723
Na_4Cl_4	3D	-1876.45384	-234.55673
Na_6Cl_6	1D	-2754.87862	-229.57322
Na_6Cl_6	2D	-2795.56555	-232.96380
Na_6Cl_6	3D	-2815.15010	-234.59584

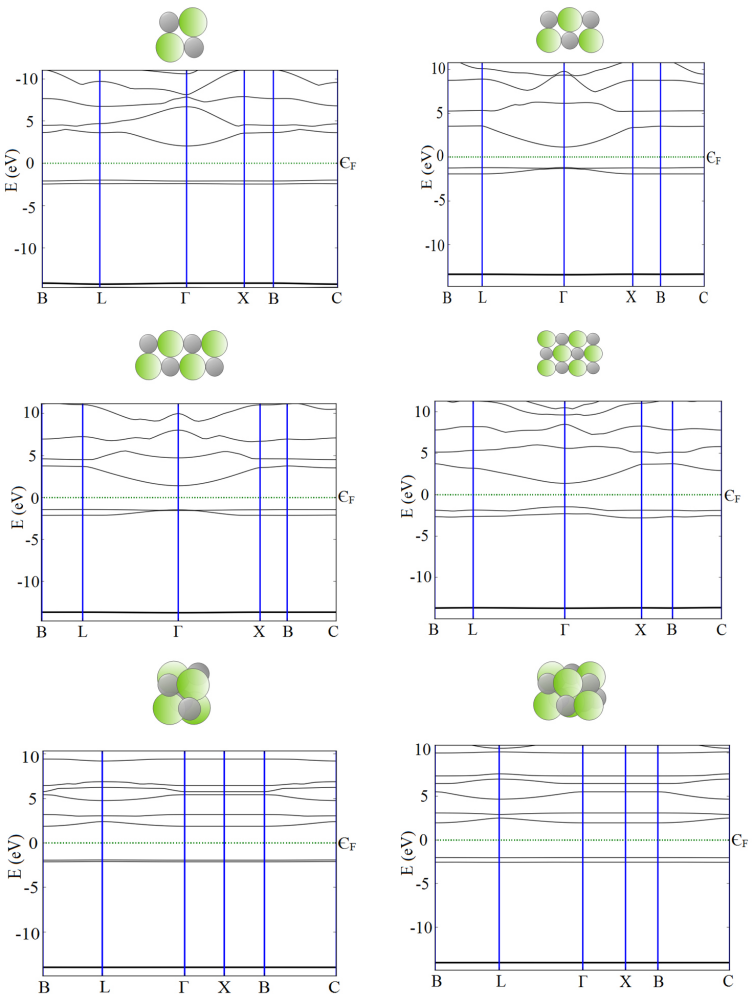

Fig. 3. Band structure of two-dimensional and three-dimensional NaCl.

4. CONCLUSIONS

In this paper, we presented the results of computer simulations of the band structure, the density of states, and the total energy of NaCl linear chains with different ion number (NaCl, Na_2Cl_2, Na_3Cl_3, Na_4Cl_4, Na_6Cl_6), depending on the geometric arrangement of ions.

Objects with a small number of atoms often exhibit thermodynamic, structural, energetic, dynamic, electronic, and chemical properties, which differ considerably from bulk materials, reflecting the finite-size of these systems. The simulation of the above-mentioned properties of NaCl chains may be useful for the calculation of energetical properties of alkali halide nanocrystals.

ACKNOWLEDGEMENTS

The authors thank Eugene Kotomin and V. Kuzovkov for fruitful discussions and valuable suggestions. A.I.P thanks A.Moskina for the technical assistance in preparation of the manuscript. A.I.P also gratefully acknowledges a project LZP-2018/1-0214 from the Latvian Council of Science for partial support.

REFERENCES

1. Lushchik, C., Kolk, J., Lushchik, A., Lushchik, N., Taiirov, M., & Vasilchenko, E. (1982). Decay of excitons into long-lived F, H and α, I pairs in KCl. *Physica Status Solidi (b)*, *114*(1), 103–111.
2. Lushchik, C., Kolk, J., Lushchik, A., & Lushchik, N. (1984). Radiational creation of Frenkel defects in KCl- Tl. *Physica Status Solidi (a)*, *86*(1), 219–227.
3. Lushchik, A. C., & Frorip, A. G. (1990). Thermalized and hot interstitial halogen ions in alkali halides. *Physica Status Solidi (b)*, *161*(2), 525–535.
4. Popov, A. I., Kotomin, E. A., & Maier, J. (2010). Basic properties of the F-type centers in halides, oxides and perovskites. *Nuclear Instruments and Methods in Physics Research Section B: Beam Interactions with Materials and Atoms*, *268*(19), 3084–3089.
5. Eglitis, R. I., Popov, A. I., & Kotomin, E. A. (1995). Computer simulations of I-center annealing in KCl and KBr crystals. Theoretical interpretation of thermostimulated experiments. *Physica Status Solidi (b)*, *190*(2), 353–362.
6. Kuzovkov, V. N., Popov, A. I., Kotomin, E. A., Moskina, A. M., Vasilchenko, E., & Lushchik, A. (2016). Theoretical analysis of the kinetics of low-temperature defect recombination in alkali halide crystals. *Low Temperature Physics*, *42*(7), 588–593.
7. Lushchik, A., Lushchik, Ch., Vasil'chenko, E., & Popov, A. (2018). Radiation creation of cation defects in alkali halide crystals: Review and today's concept. *Low Temperature Physics*, *44*, 357–367.
8. Kotomin, E., Popov, A., & Hirai, M. (1994). A contradiction between pulsed and steady-state studies in the recombination kinetics of close Frenkel defects in KBr and KCl crystals. *Journal of the Physical Society of Japan*, *63*(7), 2602–2611.
9. Kotomin, E. A., Popov, A. I., & Eglitis, R. I. (1992). Correlated annealing of radiation defects in alkali halide crystals. *Journal of Physics: Condensed Matter*, *4*(27), 5901–5910.

10. Szymonski, M., Droba, A., Struski, P., & Krok, F. (2012). Dynamics of the defect-mediated desorption of alkali halide surfaces. *Low Temperature Physics*, *38*(8), 774–778.
11. Chernov, S. A., Trinkler, L., & Popov, A. I. (1998). Photo-and thermo-stimulated luminescence of CsI—Tl crystal after UV light irradiation at 80 K. *Radiation Effects and Defects in Solids*, *143*(4), 345–355.
12. Popov, A. I., Chernov, S. A., & Trinkler, L. E. (1997). Time-resolved luminescence of CsI-Tl crystals excited by pulsed electron beam. *Nuclear Instruments and Methods in Physics Research Section B: Beam Interactions with Materials and Atoms*, *122*(3), 602–605.
13. Popov, A. I., & Balanzat, E. (2000). F centre production in CsI and CsI–Tl crystals under Kr ion irradiation at 15 K. *Nuclear Instruments and Methods in Physics Research Section B: Beam Interactions with Materials and Atoms*, *166*, 545–549.
14. Totsuka, D., Yanagida, T., Fujimoto, Y., Yokota, Y., Moretti, F., Vedda, A., & Yoshikawa, A. (2012). Afterglow suppression by co-doping with Bi in CsI: Tl crystal scintillator. *Applied Physics Express*, *5*(5), 052601.
15. Rogulis, U., Spaeth, J. M., Elsts, E., & Dolgopolova, A. (2004). Tl-related radiation defects in CsI: Tl. *Radiation Measurements*, *38*(4–6), 389–392.
16. Zorenko, Y. V., Turchak, R. M., Gryk, W., & Grinberg, M. (2004). Luminescent spectroscopy of Eu^{2+} centers in CsBr: Eu single crystals at 10–550 K. *Journal of Luminescence*, *106*(3-4), 313–320.
17. Trinkler, L. E., Trinkler, M. F., & Popov, A. I. (1993). Stimulation energy of the X-ray storage material KBr: In. *Physica Status Solidi (b)*, *180*(1), K31–K34.
18. Schweizer, S. (2001). Physics and current understanding of X-ray storage phosphors. *Physica Status Solidi (a)*, *187*(2), 335–393.
19. Popov, A. I., & Plavina, I. (1995). Photostimulated emission of KBr—In previously exposed to UV-or X-radiation. *Nuclear Instruments and Methods in Physics Research Section B: Beam Interactions with Materials and Atoms*, *101*(3), 252–254.
20. Halliday, M. T. E., Hess, W. P., & Shluger, A. L. (2015). Structure and properties of electronic and hole centers in CsBr from theoretical calculations. *Journal of Physics: Condensed Matter*, *27*(24), 245501.
21. Armington, A. F., Posen, H., & Lipson, H. (1973). Strengthening of halides for infrared windows. *Journal of Electronic Materials*, *2*(1), 127–136.
22. Kumar, A., Ravindra, N., & Rath, R. (1979). Optoelectronic properties of alkali halides. *Journal of Physics and Chemistry of Solids*, *40*(12), 1141–1142.
23. Uzi, L., Scharf, D., & Jortner, J. (1985). Electron localization in alkali-halide clusters. *Physical Review Letters, 54(16),* 1860–1863.
24. Whetten, R.L. (1993). Alkali Halide Nanocrystals. *Acc. Chem. Rev.*, *26,* 49–56.
25. Lisitsyn, V., Lisitsyna, L., & Polisadova, E. (2015). Nanodefect substructures in crystal phosphors. *IOP Conference Series: Materials Science and Engineering*, 81(1), 012020.
26. Babin, V., Elango, A., Kalder, K., Maaroos, A., Shunkeev, K., Vasilchenko, E., & Zazubovich, S. (1999). Luminescent defects created in alkali iodides by unelastic uniaxial deformation at 4.2K. *J. Luminescence, 81*, 71–77.
27. Shunkeyev, K., Sergeyev, D., Myasnikova, L., Barmina, A., Shunkeyev, S., Zhanturina, N., & Aimaganbetova, Z. (2014). Vacancy dipole currents of thermostimulated depolarization in a plastically deformed KCl crystal. *Russian Physics Journal, 57(4),* 451–458.
28. Kotomin, E. A., Kuzovkov, V. N., & Popov, A. I. (2001). The kinetics of defect aggregation and metal colloid formation in ionic solids under irradiation. *Radiation Effects and Defects in Solids*, *155*(1–4), 113–125.

29. Shunkeev, K., Sarmukhanov, E., Barmina, A., Myasnikova, L., Sagimbaeva, Sh., & Shunkeev, S. (2008). Specific features of the temperature quenching of luminescence of self-trapped excitons in alkali halide crystals under low-temperature deformation. *Phys. Solid State, 50(10),* 1799–1802.
30. Wang, F., & Landau, D.P. (2001). Efficient, multiple-range random walk algorithm to calculate the density of states. *Phys. Rev. Lett. American Physical Society*, *86*, 2050–2053.
31. Kaukonen, H.-P., Landman, U., & Cleveland, C.L. (1991). Reactions in clusters. *J. Chem. Phys*., *95*, 4997–5013.
32. Heidorn, S.-Ch., Bertram, C., Cabrera-Sanfelix, P., & Morgenstern, K. (2015). Consecutive mechanism in the diffusion of D_2O on NaCl (100) bilayer. *ACS Nano*, *9(4),* 3572–3578.
33. Hoya, J., Laborde, J.I., Richard, D., & Rentería, M. (2017). Ab initio study of F-centers in alkali halides. *Computational Materials Science*, *139*, 1–7.
34. Valeev, F., & Sherrill, C. D. (2003). The diagonal Born–Oppenheimer correction beyond the Hartree–Fock approximation. *The Journal of Chemical Physics*, *118 (9)*, 10.1063/1.1540626.
35. *Atomistix ToolKit. Manual Version 2015.1.,* 840 (QuantumWise A/S: 2015).
36. Cherepanov, A.N., & Shul'gin, B.V. (2005). Utochneniye raschetnykh znacheniy radiusov ionov shchelochnogaloidnykh soyedineniy. *Problemy spektroskopii: mezhvuzovskiy sbornik nauchnykh trudov*, Yekaterinburg, *19*, 77–86.
37. Sharma, S., Dewhurst, J. K., Lathiotakis, N. N., & Gross, E. K. (2008). Reduced density matrix functional for many-electron systems. *Phys. Rev.*, *B 78*, 201103(R).
38. Kohn, W.A., Becke, D., & Parr, R.G. (1996). Density functional theory of electronic structure. *J. Phys. Chem.*, *100,* 12974–12980.
39. Roessler, D. M., & Walker, W. C. (1968). Electronic spectra of crystalline NaCl and KCl. *Physical Review*, *166*(3), 599.

ELEKTRONISKO JOSLU STRUKTŪRAS UN STĀVOKĻU BLĪVUMA DATORMODELĒŠANA NaCl JONU LINEĀRAJĀM ĶĒDĒM

L.N. Mjasņikova, A.S. Istļaup, D.M. Sergejevs, N.N. Žanturina,
K.Š. Šunkejevs, A.I. Popovs

K o p s a v i l k u m s

Pētījumā sniegtas NaCl (NaCl, Na_2Cl_2, Na_3Cl_3, Na_4Cl_4, Na_6Cl_6) lineāro atomu ķēdes elektroniskās joslas struktūras, stāvokļu blīvuma un pilnas enerģijas pirmo principu datormodelēšanas rezultāti. Norādīto īpašību modelēšana tiek realizēta ar datora kodu Atomistix ToolKit apvienojumā ar Virtual NanoLab. Kopējā enerģija ir atkarīga no pētāmā nanoobjekta jonu skaita, bet praktiski nav atkarīga no jonu ģeometriskā izkārtojuma.

26.07.2019.

sciendo

LATVIAN JOURNAL OF PHYSICS
AND TECHNICAL SCIENCES
2019, N 4

DOI: 10.2478/lpts-2019-0025

ENVIRONMENT PROTECTION

MODEL MONITORING AND EVALUATION OF RADIOACTIVE CONTAMINATION

I. Yeremeyev[1], A. Dychko[2], V. Kyselov[1], N. Remez[2], S. Kraychuk[3], N. Ostapchuk[3]

[1] Taurida National V.I. Vernadsky University
33 Ivana Kudri, Kyiv, 04000, UKRAINE
[2] Institute of Energy Saving and Energy Management, National Technical University of Ukraine "Igor Sikorsky Kyiv Polytechnic Institute"
37 Peremohy Ave., Kyiv, 03056, UKRAINE
[3] Department of Economic Cybernetics, Rivne State University of Humanities
12 Stepana Bandery Str., Rivne, 33000, UKRAINE
aodi@ukr.net

The present paper provides the methodology of monitoring and evaluation of dynamics of radioactive contamination from radioactive waste depositories, which supposes the wide application of the fuzzy set theory results, heuristics and risk-oriented management. The developed technique is based on hybrid modelling and data mining principle and provides effective control operations, realises appropriate environmental monitoring, assures trustworthy of decision making in situations of noise, ambiguity and misrepresented data.

Keywords*: decision making, fuzzy set, heuristics, metrics, model monitoring, radioactive contamination*

1. INTRODUCTION

The problem of storage of radioactive waste is related to the necessity of defence of environment from distribution of radioactive contamination (RC) for the scopes of depositories. Migration of RC can be caused by two factors: diffusive processes, which are characterised by extraordinarily low speeds of flowing, and direct loss from depressurisation of containers caused by the consequences of natural calamities, failures or assassinations. Monitoring of RC migration should include the following activities: determination of level of contaminations in the set (critical) points, such as qualifier wells on the scopes of depository of radioactive waste (RW), tests of air and soil on directions from a depository to the dwelling arrays, areas of

rest, etc., comparison of values of contamination with the possible levels and with the levels of contamination of previous supervisions, calculation of trends, rule-making in relation to the further fate of depository (its exploitations, closing or creation of artificial protective barrier with the purpose of deceleration of RC migration).

The problem of the effective monitoring of RC is complicated due to the necessity to control the levels of contamination, which barely exceed the thresholds of sensitiveness of measuring devices, to reduce the amount of drawn samples and ambiguousness of the estimation of results. Such a procedure does not allow exposing the fact of migration of RC at the initial stages of situation. Therefore, there is a necessity to apply such approaches which allow determining motion of «spot» of RC even in similar terms.

Model monitoring of possible migration of RC, taking into account the processes of diffusion, filtration and real conditions of environment, in the affected depositories of RW zones is widely used at present time [1]. In addition, methods, being based on the use of Bayes' theorem, get wide distribution for those cases, when it is necessary to operate with the limited retrieval of data, the laws of their distribution are unknown a priori [2]. Finally, the methods of the fuzzy set theory are used, when the implementation of the probed variables can be described with the use of linguistic estimation, rather than analytically [3]–[5]. However, much of all in-use methods and approaches have one failing: they possess low sensitiveness in the conditions of normal exploitation of depositories of RW and do not allow exposing the dynamics of "spots" of contamination at the initial stages of catastrophic situations.

2. ESTIMATION OF RADIOACTIVE CONTAMINATION DYNAMICS

The aim of the research is to develop and justify an approach of objective estimation of the contamination distribution tendencies in an environment at the early stages, when changes are within the limits of fluctuations of natural background and threshold of sensitiveness of measuring devices and methods, but the presence of external factors allows supposing the latent phase of RC migration process.

As established above, monitoring is carried out under the condition when the speed of RC migration in an environment is very small. However, in case of catastrophic phenomena all changes are determined, as a rule, not after the exposure of considerable concentration of contamination (that can be already too late for making important management decisions), but on the basis of indirect (concomitant) information, for example, information about an earthquake, flood or tornado, fire or assassination, which could influence the terms of RW storage in a depository. One of the main problems of durability of depositories is seismic firmness. Its provision will be implemented both due to the proper construction of depositories and monitoring of buildings and constructions of depository (with the use of direct and mediated methods) with the purpose of exposure and removal of risk of their breakage, collection of the data about strong changes, increase of knowledge about changes in the redistribution of the main direction of motion of ground-waters, drafting of cards of seismically dangerous areas, having connection with the affected depository zone.

Sometimes the relevant monitoring parameters may not be defined and compared between each other and then it is necessary to resort to the methods of the fuzzy set theory, replacing functional dependences, the so-called functions of belonging (FB), and using linguistic variables for the aim of comparison. At the same time, variables can be divided into a few groups, for example, groups where variables are considered belonging to zero (Z), small values (S), mean values (M) and big ones (B). Then the function of belonging $\mu(x)$ to one or another linguistic variable can be presented as follows:

$$\mu(x) = \begin{cases} 0, x \le a, d \le x \\ \dfrac{x-a}{b-a}, a \le x \le b \\ 1, b \le x \le c \\ \dfrac{d-x}{d-c}, c \le x \le d \end{cases}, \tag{1}$$

where $a_i \le b_i \le c_i \le d_i$ correlate with the expert estimations of scopes, in which the proper (i-th) linguistic variables of *Z, S, M* and *B* are situated. FB *[*or $\mu(x)$*]* can be presented as in Fig. 1. Thus, if the variable of X_i takes on three concrete values, in the case of $x = X_1$, $FB_Z = 0$, and $FB_S = 0.64$ and the value of X_1 can be determined as the linguistic variable S; in the case $x = X_2$, $FB_S = 0.33$, and $FB_M = 0.76$ and X_2 belongs to the linguistic variable *M*; in the case $x = X_3$, $FB_M = 0.72$, and $FB_B = 0.33$ and X_3 belongs to the linguistic variable *M***.**

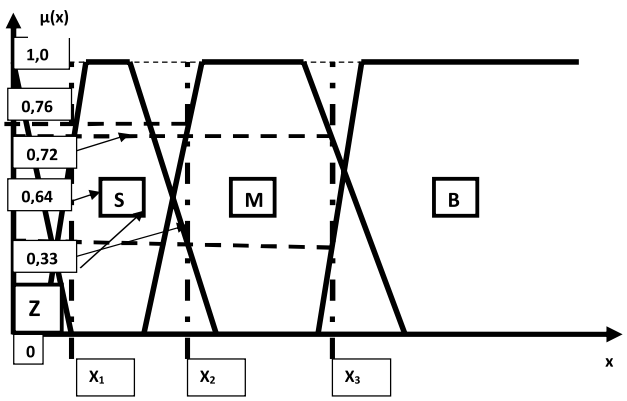

Fig. 1. Procedure of determination of belonging the concrete value to the proper linguistic variables.

During the monitoring it is also important to expose tendencies in the dynamics of RC under conditions of values of RC concentrations approximately equal to the value σ. For this purpose it is suggested to use Euclidean metrics, characterising distance between spreading of RC, characteristic for the previous cycle of measuring, and distributing of RC at the current cycle of monitoring. In the case when this metrics does not exceed 2σ, distributing is considered identical and the dynamics of

RC spot is absent, in opposite case the fact of displacement of RC spot is fixed. This approach was tested on the example of low-level radioactive contamination spot distribution compared to the sensitiveness of detectors. The contaminated area on the territory of alienation of Chernobyl NPS was inspected during a few years; thus, the tests of activity were taken in the same points annually. The information was analysed for ten points of sampling; thus, in every point executed for one hundred measuring, information about which after averaging (Table 1) and standard deviation evaluation were determined, and then the metrics for three cycles of measurement were calculated.

Table 1

Averaged Results of Three Cycles of Activity Measurement, bq/l

# sampling	1	2	3	4	5	6	7	8	9	10
1st cycle	0.507	0.57	0.6	0.6	0.6	0.6	0.6	0.6	0.62	0.6
2nd cycle	0.7	0.7	0.7	0.72	0.68	0.7	0.67	0.51	0.48	0.46
3rd cycle	1.609	1.664	1.626	1.677	1.668	1.242	0.811	0.624	0.532	0.557

Figure 2 presents comparative statistics of pair of actual values of activity distributions taking into account the values of measure of dE and 2σ for the 1st–2nd and 2nd–3rd cycles. Since Euclidian metrics between distributions of values of the 1st and 2nd cycles of measurement does not exceed the value of 2σ, dynamics of RC is considered to be absent. If Euclidian metrics between distributions of values of the 2nd and 3rd cycles of measurement substantially exceeds the value of 2σ, it confirms migration of RC spot.

3. DEVELOPMENT OF THE "DEPOSITORY – ENVIRONMENT" SYSTEM MODEL OF RADIOACTIVE STATUS MANAGEMENT

The model of the "Depository–Environment" system radioactive status management (DESRASM) should be based on the cumulative data, the knowledge base, set of rules of production, logical deduction gear and conclusion building gear by means of uncertain and incomplete input data. In other words, DESRASM should be an Expert System (ES).

Cumulative data or Data base (DB) as a rule is formed by the following components:

- background data - the monitoring points with fixed spatial coordinates and related data (number of points, date of measurement, the measurement procedure);
- parameter – defines the general activity of radionuclide's type and spectrum;
- value - defines α-, β- and γ-activity of every component of the spectrum (absolute or comparative);
- attendant factors - define the routine monitoring results or the results caused by force-majeure (earthquake, flood, man-caused ones etc.);

- comments - define the presence and nature of changes in comparison with the previous measurements, other peculiarities.

Knowledge base (KB) should save alternative models of behavior of all system components and system as a whole undervarious conditions of functioning, with different external factors and various forms and processes of RC migration.

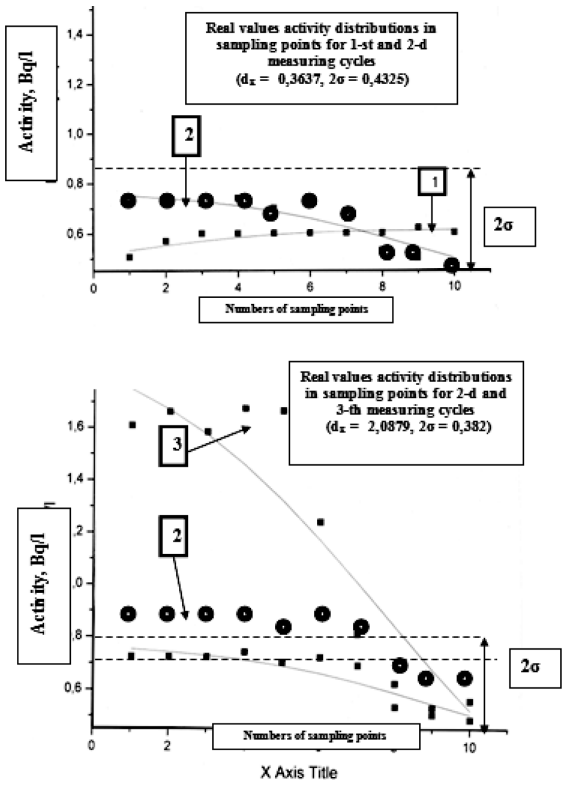

Fig. 2. Comparative statistics of pair of actual activity value distributions for the 1st-2nd and 2nd-3rd measuring cycles.

The rules of production (RP) or heuristics are formed per next sample: IF (precondition), THEN (action) [index of distinctness ID]. As the precondition the above components conjunctions may be used and action includes the components parameter value definition. For the action's ID computation, the rule's ID with the ID of those DB components related to the appropriate rule is used.

The rules may be developed on the basis of relative precondition for action of quintet parameter value awarding (the direct sequence of deduction guided by data) or proceed from action's quintet for ascertainment of those precondition quintets which shall be defined (inverse sequence of deduction which guided by the aim). The main goal is the accumulation of possible preconditions and possible actions. Index of distinctness may be computed by ID precondition, ID rule and output ID of DB. ID precondition is determined by the least of the ID statements which are composed in the precondition.

Obtained values are multiplied by rule ID (for the part of action) and then the resulting index (RI) is arrived. If the quintet is not shaped for this moment, RI may play the role of quintet ID. In this case with the output index (OI) the values of ID are found by next procedure:

$$\begin{aligned} ID &= OI + RI\left(1 - OI\right), RI, OI \rangle 1 \\ ID &= -\left(\left|RI\right|\left(1 - \left|OI\right|\right)\right), RI, OI \langle 1 \\ ID &= \frac{\left|OI\right| + \left|RI\right|}{1 - \min\left\{\left|OI\right|, \left|RI\right|\right\}}, RI, OI \langle 0 \end{aligned} \tag{2}$$

Checking of the model may be implemented by its sensitivity to parameter deviations and adjustment of some parameters for the purpose of accordance of the predicted extrapolation and real measurements of RC values. After this adjustment the RC spot dynamics modeling is implemented along the period of depository functioning. Another step is also permissible (if there are several models of RC spot dynamics): implementation of concurrent modeling by several models and use of the model which has the minimal metric of predicted distribution of RC spot relative to the real distribution.

One of the main problems of depository impermeability is the seismic resistance, which is realized by:

- adequate depository design and by means of installations;
- design monitoring (with the help of direct and mediate methods) for the exposure and elimination of the danger of their destruction;
- the great landslides data collection;
- knowledge level increasing about deviations in the main direction of subterranean waters redistribution;
- drawing up the seismic dangerous maps connected with the depository's influence zone.

Mentioned monitoring in routine process analyzes periodically the depository functioning conditions. However in cases of natural or man-made accidents, which may influence the depository, condition of the code of causal monitoring should be activated.

The monolithic constructions as depositories theoretically may be checked by their reaction on the external vibrations. Their natural frequency and external source vibration absorption factor may be used for evaluation. As several authors claim [6]: the more damages - the less (monotonously) natural frequency, and external vibration absorption arises from the beginning and then – decreases. Hence, the alternations in construction inflexibility and especially vibrations may be used as indices of structural damage. Such research should be carried out after every earthquake which is fixed in-situ of depository. It is also necessary to fulfill some analytical inspection, which supposes the careful study of initial constructive calculations, designed specifications, and extra structural analysis combined with field observations and test data.

The real depository status may be found out by taking into account the accumulated effect of seismic stresses (landslides, fractures, shocks). Therefore, it is necessary:

- to determine the frequency and strength of shocks in-situ of depository over the entire observation period and on the base of these data to formulate the forecast in the future;
- to simulate the influence of accumulated landslides, fractures and shocks on the depository constructions from the point of view of the probability of structure changes in depository walls and bottom, which may stipulate the formation of microcrack net, summary area of which promotes the RC component departure (migration).
- to determine the threshold exceeding of which guarantees more than 50% probability of microcrack net rise.

After listed steps it is necessary to equip the stations for depository status monitoring by accelerometers which are connected with automated monitoring system (AMS).

Inadequacy of RC component expansion optimal model may be determined by several reasons:

- Truncation (on purpose of simplification) of separate member (regarded as inessential) equation, which describes the processes in depository and environment;
- Assumption of invariability of separate arguments or variables in specific prescribed conditions;
- Selection of unequal (to real conditions) values of coefficients and parameters;
- Combined action of steps indicated above.

To avoid the errors caused by the above-mentioned reasons, it is necessary to use several alternative models. The simulation may be implemented simultaneously by using several (k) models with the same input data. The object of simulation is getting the spectral characteristic in N points of checking at the predetermined time of forecast. When that time comes, it is necessary to compare the simulation forecasting results x_n^i with the real RC component distribution in points of monitoring by means of metrics calculation. The metrics is characterised by the difference of simulation results from real RC component distribution in points of checking. Metrics may be two-dimensional and presented for the k models as follows:

$$d_{\substack{iE \\ i=\overline{[1,k]}}}\left[f^f, f^i\right] = \sqrt{\frac{1}{n-1}\sum_{n=1}^{N}\left(x_n^f - x_n^i\right)^2}. \tag{3}$$

The optimal model *Mopt* must correspond to the next condition:

$$dMopt = \min\left[d1E, d2E, \ldots dkE\right]. \quad (4)$$

The decision-making procedure (DMP) during the depository status monitoring, i.e. elaboration of either one or another strategy, may be implemented on the basis of the following operator:

$$DMP :\rightarrow K\left\{A, TA, E, PA, R\right\}, \quad (5)$$

where A – a set of alternatives, i.e., decision variants which correspond to certain conditions (task limitations) and achieve the aim. These alternatives are formulated in advance (for example, by decision making person (DMP) or decision making system (DMS)). Each of them has a typical set of "trifles" – TA – which under defined conditions may initiate some unwanted evolution of an event, where E – environment of DMP task, i.e., the conditions under which the decision making is implemented (including the functioning conditions of specific technical-organisational system). This environment should be necessary taking into account formalization and solution of the task. PA – priority, established by DMS and related to the main criteria, advantages and disadvantages of some alternatives from the point of view of specific reality, relevant to specific RW depository or environment conditions and factors in force, as well as from the point of view of taking into account suitable "trifles". This allows implementing single-minded selection of members from A-set corresponding to the R-procedure over the A-set, in which connection R is characterised by the type of DMP (looking for the most inviting alternative, separation of the set of alternatives which are not dominating, regulating of alternatives' set which are admissible etc.). Here "trifle" is the factor, which under specific circumstances (as a rule extreme), determines the management strategy in close conditions especially at information imperfection and fuzziness as well as the time lack during DM (under normal conditions this factor as a rule "hides behind the background", i.e. "conceals" behind more meaningful under these condition factors).

DMS priority system is the decisive component of DM. However, this system snaps into action generally on the assumption of transparency and unambiguity criteria, which define the desired optimal alternative. Under real conditions, PA is frequently characterised by conceptual imperfection ("opacity"), lack of distinct boundaries (fuzziness), which prevent from confident selection of a concrete alternative among the forward-looking (from the point of view of DMS) alternatives. In these cases the next approach may be used.

All the data that characterise specific alternatives are formed in a way of "spectrum", in which the every component is situated on the fixed place ("strict format"). Connection of the amplitude of "spectral line" (or the inverse value if the amplitude is a negative trait of alternative) characterises a relative value of a corresponding component, which may be presented as part of maximum possible value or may be characterised as some notion from possibility theory's field (for example "relevant", "conformal", "identical" and so on, which may also be presented as numbers from 0 to 1). In this case, the absence of a spectrum component in real

characteristic is reflected as a component with the zero amplitude. For example, the component that does not have any relation to the problem is characterised as 0; the component that has some relevancy to the problem is characterised as 0.25; the component that has considerable relevancy to the problem is characterised as 0.5; conformal – as 0.7 and identical – as 1.00. The curve that bends the "ideal" spectral characteristic (i.e. characteristic which has only the "one's" spectral values) may be represented as a straight line parallel to abscess axis. The curves which bend the real spectral characteristics differ from "ideal" one. As a measure of discrepancy of the real and "ideal" characteristics the Euclidean metrics (which is the reciprocal to function affiliation) may be used:

$$\frac{D_r}{r=1,R} = \sqrt{1/\left[j-1\right] \sum_{j=1,n} \left[1-x_{rj}\right]^2}, \tag{6}$$

where j – total amount of spectral lines including the "trifle spectrum", R – total amount of alternatives that are examined (correspondingly j and r – numbers of spectra and alternatives which are examined at the given moment), x_{rj} – numeric values of j-th spectral line of the r-th alternative.

Under these circumstances, the optimal alternative should correspond to the following condition:

$$Dr(opt) = \min\left[D1, D2, ...DR\right]. \tag{7}$$

In case of alternative ranking procedure accomplishment (for example, separation of alternatives which have the metrics out of permissible limits or linear regulating of alternatives which are acceptable in principle) these procedures may be accomplished by the algorithm:

$$\begin{aligned} &Dr(opt) :\rightarrow 1, ...k :\rightarrow k \pm 1, ...k \neq R \\ &Dr(range) = Dr(opt) :\rightarrow Dk \leq D\max, k = R \rightarrow STOP \\ &k = 1 :\rightarrow Dk \geq D\max \rightarrow STOP \end{aligned} \tag{8}$$

In other words, the k-th optimal alternative determines successively from alternative set in which instead of each earlier determined optimal (with minimal metrics) spectral line substitutes its maximum (single or "1") value $Dr(opt) : \rightarrow 1$. If the next metrics is equal or exceeds acceptable bounds $Dk \geq Dmax$ the subsequent search is ceased as soon as the quantity of successive fixed alternatives runs up to quantity of alternatives in A-set, i.e., when $k = R$. The alternatives fixed by such an approach are ranked automatically according to monotonous increasing metrics values and get the respective numbers (k).

The proposed approach is sufficiently general and effective way of optimal alternative (or alternatives' subset which is acceptable in principle for the decision making under specific conditions) searching. It may be used if there are general set

of possible alternatives under circumstances, which are characterised by slipshod depending on several factors and hence are not sufficiently "transparent" as to the DMS so as to independent experts, invited especially for optimal alternative selection.

4. CONCLUSIONS

1. Definition of monitoring parameters under conditions of fuzzy and incomplete data implies determination procedure of belonging of the concrete value to the proper linguistic variables and estimation of scopes.
2. Euclidean metrics characterising the distance between spreading of radioactive contamination, characteristic for the previous cycle of measurement and its distribution at the current cycle of monitoring is used for radioactive spot dynamics reliable evaluation.
3. The model of the "Depository–Environment" system radioactive status management should be based on the cumulative data, the knowledge base, set of rules of production, logical deduction gear and conclusion building gear by means of uncertain and incomplete input data.
4. Checking of the developed model is implemented by definition of its sensitivity to parameter deviations and their adjustment for the purpose of accordance of the predicted and real measurements of contamination.
5. Implementation of the developed procedures ensures the effective and reliable estimation of the state of environment in zone of depository of radioactive waste and prognostication of radioactive contamination dynamics.

REFERENCES

1. Yu, C., Zielen, A.J., Cheng, J.-J., LePoire, D. J., Gnanapragasam, E., Kamboj, S. … Peterson, H. (2001). *User's manual for RESRAD version 6. Environmental assessment division*. Argonne National Laboratory. United States Department of Energy. Available at: http://www.doe.gov/bridge.
2. Hoeting, J. A., Madigan, D., Raftery, A. E., & Volinsky, C. T. (1999). Bayesian model averaging: A tutorial. *Statistical Science, 14*(4), 382–417.
3. Yeremeev, I. S., & Dychko, A. O. (2016). The problem of uncertainty in monitoring the environment. *Systems of Information Processing, 6,* 45–47.
4. Yeremeyev, I. S. (2008). Decision-making problems during monitoring of environment in the conditions of uncertainty. In: *Proceedings of 10th International Scientific and Technical Conference* "*Systems Analysis and Information Technologies".* May, 20-24, 2008. NTUU KPI: Kyiv, 187. Available at: http://sait.kpi.ua/books/
5. Orsoni, A., Karadimas, N. V. (2006). Municipal solid waste generation modeling based on fuzzy logic. In: *Proceedings of 20th European Conference on Modelling and Simulation*. May, 28-31, 2006. Digitaldruck Pirrot GmbH: Bonn, 309-314.
6. Yager, R. R., & Colledge, I. (eds.) (1982). *Fuzzy set and possibility theory. Recent developments.* Pergamon Press: New York.

RADIOAKTĪVĀ PIESĀRŅOJUMA UZRAUDZĪBA UN NOVĒRTĒŠANA

I. Jeremejevs, A. Dičko, V. Kiselovs,
N. Remezs, S. Kraičuks, N. Ostapčuks

K o p s a v i l k u m s

Rakstā piedāvāta radioaktīvo atkritumu glabātuvju radioaktīvā piesārņojuma dinamikas uzraudzības un novērtēšanas metodoloģija, kas paredz izplūdušo kopu teorijas rezultātu, heiristikas un uz risku orientētas vadības plašu izmantošanu. Izstrādātās metodes pamatā ir hibrīda modelēšana un datu izraces principi. Metode nodrošina efektīvas kontroles operācijas, atbilstošu vides uzraudzību, kā arī uzticamu lēmumu pieņemšanu trokšņu, neskaidrības un nepareizi attēlotu datu gadījumā.

09.07.2019.